Tide and Surge Propagation Off-Shore in the Dowsing Region of the North Sea

D. T. Pugh and J. M. Vassie

UDC 551.466.733: 551.466.78: 551.466.75; British coast, Marsden Square 21630

Summary

A year of simultaneous current and water level measurements at the Inner Dowsing light tower, 16 km off the Lincolnshire coast, has been analysed to investigate the tidal and shallow-water tidal components and the non-tidal water movements. These data are used in conjunction with coastal and other off-shore observations to give a detailed description of the actual off-shore tide and surge propagation in this complex region. The results are compared with analyses of elevation data elsewhere along the British coast of the North Sea.

The principal tidal constituents are obtained from analysis of the year of data and from separate monthly analyses: the variability of these monthly analyses gives estimates of the errors involved when analysing data where only a single month is available. The year of current meter observations is used to determine the amplitude and phase relationship between neighbouring tidal constituents which are not separable from shorter periods of data. These relationships are close to those in the elevations. For the M_2 constituent there is an annual modulation which is coherent along the length of the British coast of the North Sea, and which is substantially larger than the modulation in the astronomical forces. Some insight into the behaviour of tides in the vicinity of the Wash is obtained by representing each constituent as the sum of a progressive and a standing wave. At the Inner Dowsing the influence of the Wash is apparent. Cotidal and coamplitude charts are plotted for the constituents O_1, K_1, N_2, M_2 and S_2.

Similar charts are plotted for the shallow-water tidal constituents M_4, MS_4 and M_6. At the Inner Dowsing the sense of rotation of all the shallow-water current ellipses is clockwise and this is in the opposite sense to the ellipses for the astronomical tides which rotate anticlockwise. This is shown to be due to the non-rectilinear direction of the flood and ebb currents, a phenomenon which also explains the relatively greater importance of shallow-water tides in the currents than in the elevation.

Non-tidal residuals at the Inner Dowsing are not markedly smaller than at coastal stations within the Wash. For low-frequency residuals the coherence between coastal and off-shore measurements is very high, but this coherence is reduced at higher frequencies. Long-period oscillations of water level are spread across the low frequency spectrum with peaks at periods of 40 and 70 hours. Wave propagation at non-tidal frequencies is from north to south, as for the tidal waves. At the tower there is a small but significant interaction between tides and surges. The statistical distribution of residual amplitudes is closely normal for the north-south component of current, but less so for the elevations and for the weaker east-west current component.

Energy fluxes are in the direction of the progressive wave propagation from north to south. Of the total energy flux 87.5 % is accounted for by the M_2 constituent, and only 0.35 % is due to long-period surges. There is no evidence of a phase adjustment between elevations and currents to accommodate the enhanced energy dissipation at Spring tides.

Ausbreitung von Gezeiten und Fernwellen vor der Küste in der Dowsing Region in der Nordsee (Zusammenfassung)

Über den Zeitraum von einem Jahr wurden am Inner Dowsing-Leuchtturm, 16 km vor der Küste von Lincolnshire, gleichzeitig Strom- und Wasserstandsmessungen durchgeführt. Diese Messungen sind analysiert worden zur Untersuchung der Partialtiden und der Seichtwassertiden sowie der nicht von Gezeiten herrührenden Wasserbewegungen. Diese Daten werden zusammen mit Beobachtungen an der Küste und anderen Gebieten vor der Küste benutzt für eine ausführliche Beschreibung der tatsächlichen Ausbreitung der Gezeiten und der Fernwellen in diesem komplexen Gebiet. Die Ergebnisse werden verglichen mit Analysen von Wasserstandsdaten an anderen Stellen entlang der britischen Nordseeküste.

Man erhält die Stammtiden aus der Analyse der während des Jahres gesammelten Daten und aus getrennten monatlichen Analysen: Die Abweichungen dieser monatlichen Analysen voneinander geben Anhaltspunkte bezüglich der Fehler, die auftreten bei Analysen, bei denen nur Daten von einem einzigen Monat vorliegen. Die während des Jahres erhaltenen Strommeßdaten werden benutzt zur Bestimmung der Amplituden- und Phasenbeziehungen zwischen benachbarten Tiden, die bei kürzeren Datenperioden nicht zu trennen sind. Diese Beziehungen sind sehr ähnlich denen bei den Wasserständen. Für die M_2-Tide gibt es eine jährliche Modulation, die die ganze britische Nordseeküste entlang zusammenhängend ist und die wesentlich größer ist als die Modulation der astronomischen Kräfte. Aufschluß über das Verhalten der Gezeiten in der Nähe des Wash wird erhalten durch Darstellen jeder Gezeit als Summe aus einer fortschreitenden und einer stehenden Welle. Beim Inner Dowsing tritt der Einfluß des Wash offensichtlich zutage. Gezeiten- und Gezeitenstromkarten werden gezeichnet für die Tiden O_1, K_1, N_2, M_2 und S_2.

Gezeitenkarten werden gezeichnet für die Seichtwassertiden M_4, MS_4 und M_6. Beim Inner Dowsing ist die Drehrichtung aller Seichtwasser-Stromellipsen im Uhrzeigersinn, im Gegensatz zu den Ellipsen für die astronomischen Tiden, die im umgekehrten Uhrzeigersinn drehen. Es wird dargelegt, daß dies darauf zurückzuführen ist, daß die Richtung der Flut- und Ebbströme nicht entgegengesetzt ist, ein Phänomen, das auch eine Erklärung ist dafür, daß Seichtwassertiden von relativ größerer Bedeutung für die Ströme sind als für die Wasserstände.

Restströme am Inner Dowsing sind nicht wesentlich kleiner als an den Küstenstationen im Wash. Bei niederfrequenten Reststrőmen ist der Zusammenhang zwischen Messungen an der Küste und küstenfernen Messungen sehr groß, aber dieser Zusammenhang wird bei höheren Frequenzen geringer. Langzeitschwankungen des Wasserstandes erstrecken sich über das niederfrequente Spektrum mit Spitzenwerten bei Perioden von 40 und 70 Stunden. Wellen, die nicht von Gezeiten verursacht werden, breiten sich von Norden nach Süden aus wie die Gezeitenwellen. Am Leuchtturm gibt es eine geringe aber signifikante Wechselwirkung zwischen Gezeiten und Fernwellen. Die statistische Verteilung der Rest-Amplituden ist annähernd eine Normalverteilung bei der Nord-Süd-Stromkomponente, aber nicht bei den Wasserständen und bei der schwächeren Ost-West-Komponente.

Der Energiefluß geht in der Richtung der fortschreitenden Wellenausbreitung von Norden nach Süden. Von dem Gesamt-Energiefluß sind 87,5 % der M_2-Tide zuzuschreiben und nur 0,35 % den Langzeit-Fernwellen. Es liegen keinerlei Anzeichen vor für eine Phasenangleichung zwischen Höhe und Strömung, um die gesteigerte Energieauflösung bei Springtiden zu erklären.

Propagation de la marée et de l'onde de marée au large de la région Dowsing dans la mer du Nord (Résumé)

Des mesures du courant et du niveau d'eau près du phare "Inner Dowsing", qui est situé à 16 km au large de la côte du Lincolnshire, effectuées simultanément

pendant une année, ont été analysées pour étudier les composantes de la marée et de la marée due aux petits fonds, ainsi que des mouvements d'eau non dus à la marée. Ces données sont utilisées conjointement avec des observations côtières et au large pour donner une description détaillée de la propagation effective de la marée au large et de l'onde de marée dans cette région complexe. Les résultats sont comparés avec des analyses du niveau de la mer dans d'autres parties de long de la côte britannique de la mer du Nord.

On obtient les composantes harmoniques principales par l'analyse des données recueillies pendant une année et par des analyses mensuelles séparées. La variabilité de ces analyses mensuelles est un indice des erreurs qui se produisent dans des analyses où il n'y a que des données d'un seul mois. Les mesures de courant effectuées pendant une année sont utilisées pour déterminer les relations d'amplitude et de phase entre des marées avoisinantes qui ne sont pas séparables en cas de périodes de données plus courtes. Ces relations ressemblent beaucoup à celles dans les niveaux d'eau. Pour la constante harmonique M_2 il y a une modulation annuelle qui est cohérente le long de la côte britannique de la mer du Nord et qui est beaucoup plus importante que la modulation dans les forces astronomiques. On obtient des éclaircissements concernant le comportement des marées au voisinage du Wash, en représentant chaque constante harmonique comme la somme d'une onde progressive et d'une onde stationnaire. A l'Inner Dowsing, l'influence du Wash est nettement apparente. Des cartes donnant les lignes cotidales et coamplitudes sont construites pour les constantes harmoniques O_1, K_1, N_2. M_2 et S_2.

Des cartes analogues sont construites pour les constantes harmoniques M_4, MS_4 et M_6 de la marée due aux petits fonds. A l'Inner Dowsing, le sens de rotation de toutes les ellipses de courant en eau peu profonde est en sens des aiguilles d'une montre, ce qui est en sens inverse aux ellipses pour les marées astronomiques qui tournent en sens inverse des aiguilles d'une montre. On démontre que cela est dû à la direction opposée du courant de flot et du courant de jusant, un phénomène qui explique également que l'importance des marées dues aux petits fonds est relativement plus grande pour les courants que pour les niveaux d'eau.

Des courants résiduels non dus à la marée à l'Inner Dowsing ne sont pas remarquablement moindres que ceux aux stations dans le Wash. Pour les courants résiduels de basses fréquences la cohérence entre les mesures côtières et les mesures effectuées au large est très grande, mais cette cohérence est réduite dans des plus hautes fréquences. Des oscillations à long terme du niveau de la mer sont distribuées – travers le spectre de basses fréquences avec des valeurs maxima à des périodes de 40 et 70 heures. La propagation d'ondes – des fréquences non dues à la marée se produit du nord au sud, comme pour les ondes marée. Au phare "Inner Dowsing" il y a une interaction peu importante mais significative entre marées et ondes de marée. La distribution statistique des amplitudes résiduelles est à peu près une distribution normale pour la composante nord-sud du courant, mais elle l'est moins pour les niveaux d'eau et pour la composante plus faible est-ouest du courant.

Des flux d'énergie se produisent dans la direction de la propagation de l'onde progressive du nord au sud. Du flux total d'énergie, 87,5% sont dus à la composante M_2, et seulement 0,35% sont dus à des ondes de marée à long terme. Il n'y a pas évidence d'une assimilation de phase entre les niveaux d'eau et les courants pour expliquer l'accroissement de la dissipation d'énergie pendant des marées de vive eau.

Notation

d mean water depth

g phase angle of a harmonic tidal constituent relative to the phase of the equilibrium tide at the Greenwich meridian, subscripted:

ζ an elevation constituent
u an east-west current constituent, east-going positive
v a north-south current constituent, north-going positive
p a progressive wave element
st a standing wave element
m the principal lunar constituent M_2
s the principal solar constituent S_2
$'$ a current constituent

g unsubscripted – gravitation acceleration
h mean solar longitude
H amplitude of a harmonic constituent of elevation
K a dimensionless frictional stress coefficient
O instantaneous observed elevation or current component consisting of:
T the tidal element
and S the non-tidal element
Q instantaneous current speed
U amplitude of a harmonic constituent of the east-west current component
u instantaneous east-west current component
V as above for the north-south current component
v instantaneous north-south current component
$V(M_2)$ a nodal correction term for the M_2 constituent
W amplitude of a harmonic constituent of a general current component
ζ instantaneous water level relative to mean level
θ current direction measured positive anticlockwise from geographic east
λ direction of progressive wave component
ρ sea-water density
σ angular speed of a harmonic constituent in degrees per hour
φ direction of standing wave component, positive for flow on the falling tide

Introduction

The development of realistic theoretical and numerical models of sea dynamics requires measurements of off-shore elevations and currents; however, until quite recently, such measurements were rare. With the advent of reliable recording current meters and of sea-bed pressure gauges, records extending over a lunar month, an optimum period for tidal analysis, are feasible. Nevertheless, the deployment of these instruments requires specialised ships so that much longer periods of observations, involving a series of deployments, may be prohibitively expensive. Longer periods of observations provide better spectral resolution. It is possible to assess the reliability of tidal constituents determined from a single month of data, and also to study meteorological effects in more detail. Therefore, the use of permanent off-shore structures, such as oil and gas production platforms, on the continental shelf for monitoring currents and elevations over long periods is an attractive alternative.

When, in 1971, the Trinity House Lighthouse Service planned the replacement of the Inner Dowsing Light Vessel by such a permanent platform, it was decided to use it for a pilot experiment prior to more ambitious instrumentation of other rigs. The plan was to install a pneumatic water-level gauge, and to measure currents over a period of at least a year. The Inner Dowsing Light Tower, situated 16 km off the Lincolnshire coast, became operational in September 1971. The pneumatic water-level gauge began recording in October 1971; current meter measurements were made from February 1972 until November 1973.

Preliminary analyses of the Inner Dowsing observations suggested that it would be more meaningful to consider them together with observations made elsewhere in the Dowsing region, and in some cases from elsewhere along the British coast of the North Sea.

The end of this period of current measurements at the Inner Dowsing coincided with the Joint North Sea Data Acquisition Programme (1973), which included measurements of currents, bottom pressures and coastal elevations at other sites in the region. Other measure-

ments, made during 1972 and 1973 as part of the Wash Water Storage Scheme, were also available, as were measurements from gas production rigs in the Shell-Esso field, made by the University of East Anglia and the Ministry of Agriculture, Fisheries and Food. These measurements are used to investigate the dynamics of water movements in the region. Fig. 1 shows

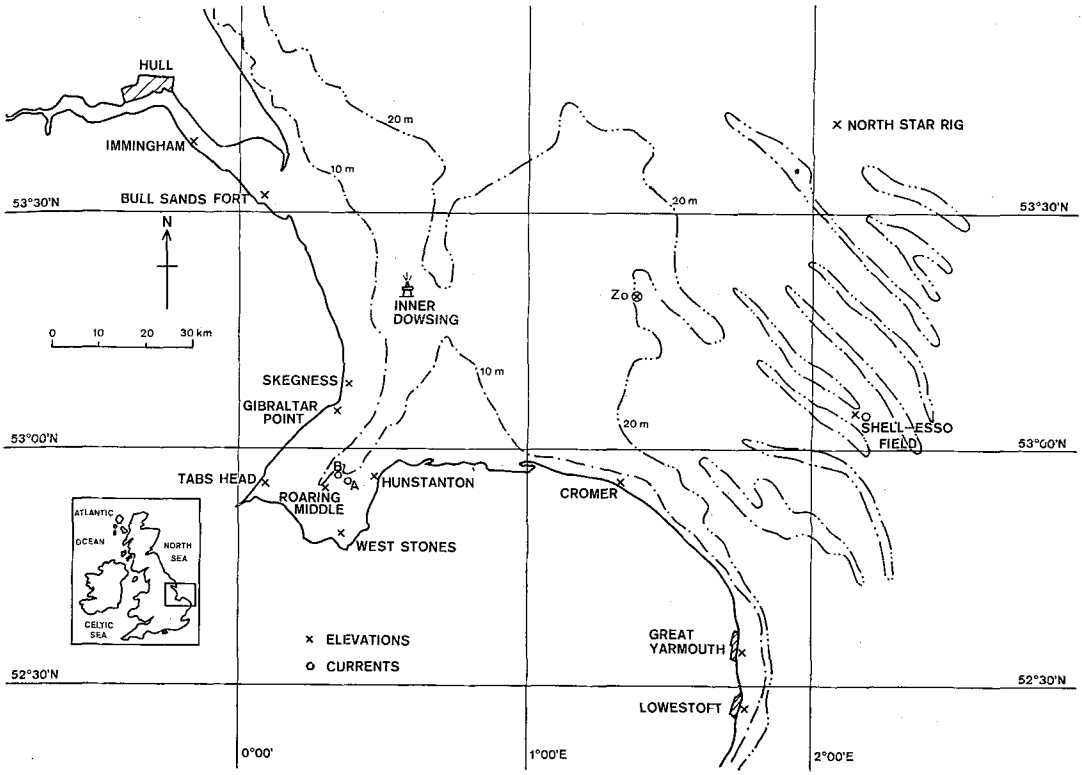

Fig. 1. Map showing the locations of measurements in the Dowsing region of the North Sea. The 10 m and 20 m depth contours relative to Admiralty chart datum are plotted

the locations of these measurements, and Table 1 gives details of the instruments and of the periods of observation.

This paper presents the results of these investigations in turn for the astronomical tides, the shallow-water tides, and the meteorological residuals.

In each case the spectroscopy of the Inner Dowsing data is considered prior to a discussion of the regional dynamics. The final section concerns the fluxes of energy in the region. However, we begin with details of the instrumentation of the Inner Dowsing Tower.

Instrumentation of the Inner Dowsing Tower

Water levels were measured using a pneumatic pressure system with a Neyrpic chart recorder. The advantages of pneumatic systems have been discussed elsewhere (Pugh [1972]) but the particular advantages which applied here were:

a) that the underwater parts of the equipment are cheap and easily repaired, and

b) the datum level is stable and clearly defined.

Nylon pressure tubing was strapped to the tower (Fig. 2) while it was still undergoing constructional modifications at Hartlepool, prior to being towed to the site. Two independent pressure point systems were fitted as a precaution against damage. In June 1972 the tube normally used was accidentally cut by divers, but only 18 hours of data were lost before the reserve pressure point was connected. Apart from this failure, the record is continuous until

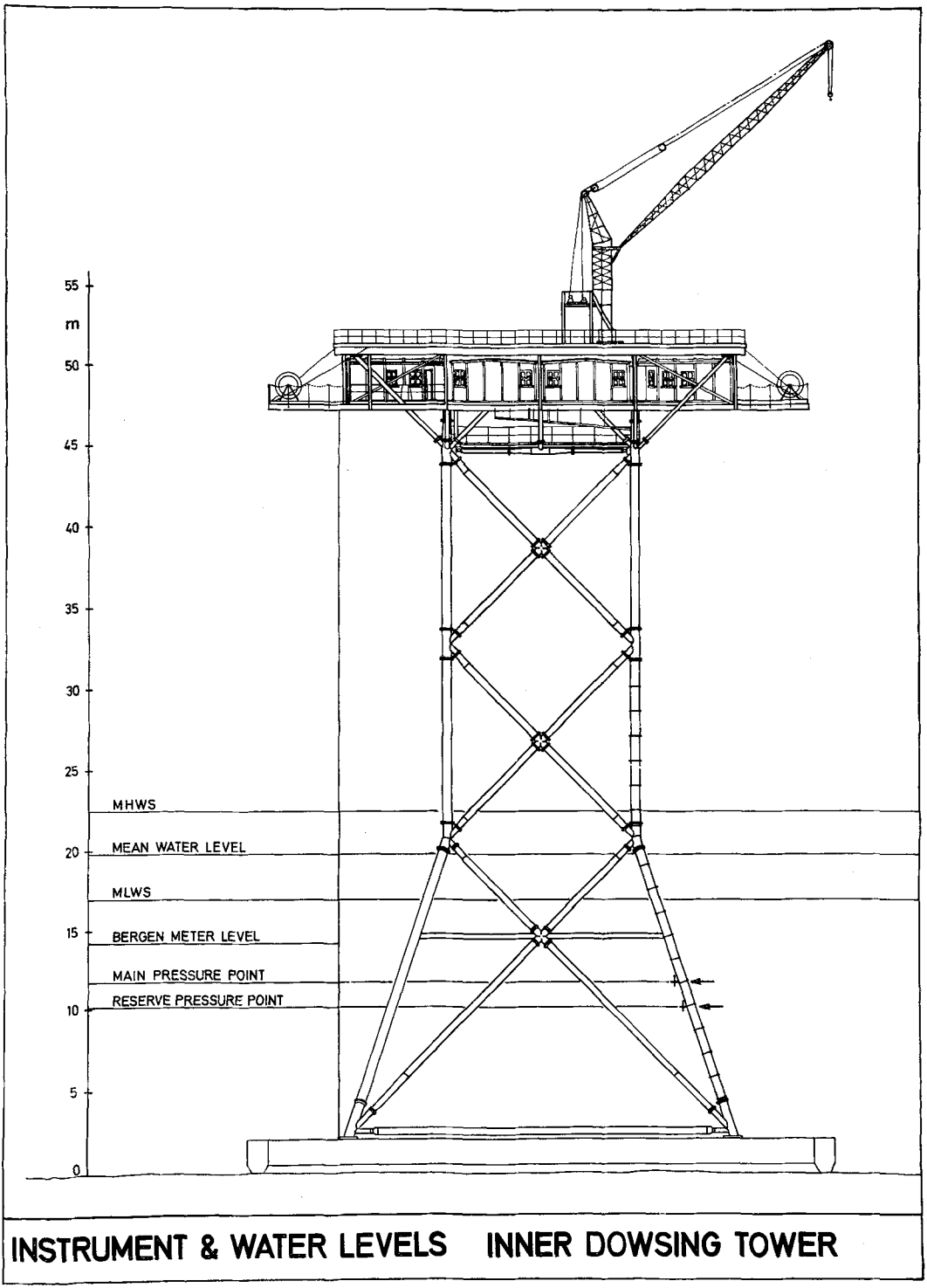

Fig. 2. The Inner Dowsing Light Tower showing instrument levels and approximate tidal water levels

January 1974, when both tubes were damaged. The gauge was restarted in August 1974. The tower is permanently manned by Trinity House staff who are responsible for the routine operation of the gauge. The chart readings were corrected in the usual way (Pugh [1972]) for the effects of waves, for chart calibration, for tube pressure gradient and for water density. In this case, because the recorder was mounted 35 m above the gas outlet datum, a correction for the static pressure head in the connecting tube was necessary. The accuracy of the system has been shown to be approximately 0.02 m. Our experience with this installation has shown that a pneumatic system is well suited for general use on off-shore structures.

Measuring the currents was more difficult. Preliminary tests showed that the effects of the tower structure were significant in the bottom 10 metres because of turbulence induced by the cruciform which forms the base of the tower. The position of minimum disturbance was found to be underneath the platforms protruding at the accommodation level (Fig. 2). A meter was suspended from the South-west platform on a wire which was tensioned by a 180 kg weight. A hand winch was available for lowering and raising the meter which was positioned 14 m above the sea bed. Aanderaa recording current meters were used, with the sampling interval set to 10 minutes. A single meter was normally left in position for 8 weeks and over the 21 month recording period 13 deployments were made. Visiting the tower, even infrequently, proved difficult. The regular supply and relief helicopter visited every four weeks, but did not stay long enough for the change over of meters – about four hours work – so that it was often necessary to commission an extra flight. To investigate further the effects of the structure on the current field around the tower, accurate visual measurements of the direction of surface flow were made from the platform, over the current meter position and over a position on the opposite side of the tower. For the north-going flow the direction measurements from opposite sides of the tower agreed to within 6°, and to within 3° for the south-going flow.

Simultaneous readings by the recording current meter were found to be rotated in an anticlockwise sense by 7° for the north-going flow and 10° for the south-going flow. One explanation of this difference is a current direction which is depth dependent, but this is unlikely as the direction fin of the instrument was frequently visible during the observations, and was aligned closely with the surface flow. More probably the permanent magnetic field of the tower distorts the geomagnetic field locally, so affecting the current meter reference direction. At the level of the upper deck the magnetic field direction was found to vary with position from 340°T to 370°T, while the local geomagnetic field bears 353°T. However, because we were unable to make direct measurements of the magnetic field at the actual current meter compass location, the currents were processed assuming an undistorted field. The first stage of this processing was to convert the recorded counts to values of current speed and direction using laboratory calibrations. These were then edited and resolved into north-south and east-west components. The ten minute values were corrected for timing errors and converted to hourly values using a low-pass smoothing filter.

Henceforth, unless otherwise stated, throughout this paper, the positive u component is directed towards the east and the positive v component is directed towards the north. Directions are measured positive in an anticlockwise direction from east. Particular days are specified in terms of the year and day number within that year (e.g. January 1st 1973 appears as 1/73).

Spectral distribution of elevation and current variance at the Inner Dowsing

The period of elevation observations from 64/72 to 63/73 was analysed using a standard least-squares technique, for 102 harmonic constituents. Current meter data, resolved into north-south and east-west components were similarly analysed for the period 57/72 to 78/73 with a gap from 308/72 to 340/72. The extreme elevations for the year were at 3.18 m and −3.41 m relative to the mean sea level, while the maximum flood (south-going) and ebb (north-going) currents were 1.42 m s^{-1} and 1.10 m s^{-1} respectively. The currents were predominantly along an approximately north-south axis. The total variances summarised in Fig. 3 give a measure of the relative contributions to the observed elevations and currents from the different frequency bands for a lunar month.

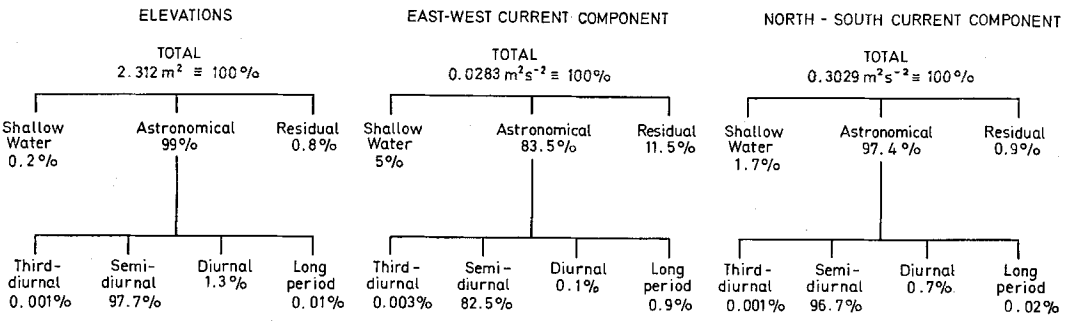

Fig. 3. Block diagram showing the distribution of variance in the current and elevation measurements at the Inner Dowsing, day 91/72 to day 119/72

For the elevations and for the dominant north-south currents almost all of the variance is at the astronomical tidal frequencies, with less than 1 % in both cases in the surge residuals. However, the shallow-water terms are relatively more important for the currents than for the elevations. The east-west component of current has a much smaller amplitude than the north-south component and the analysis is affected more by noise, so that 11.5 % of the total variance is not at tidal frequencies, and 5 % of the remainder is at shallow-water tidal frequencies.

For the complete year of data the residual variance in the elevations is 0.7 % of the total variance, which is almost the same as for the month. For the currents the residual variances over the year are 18.8 % in the east-west component and 2.9 % in the north-south component, significantly larger than for the month. This is because the harmonic constituents for the currents are less stable than those for the elevations.

The results of these analyses are now discussed for the astronomical tides, the shallow-water tides and for the non-tidal residuals in turn.

The astronomical tides

We begin by discussing the harmonic constituents of elevations and currents determined at the Inner Dowsing, and their variability from month to month. The relationships between some neighbouring constituents in both the equilibrium tide and the observed elevations and currents are also discussed. We then investigate the relationship between the tides at Lerwick and those at the Inner Dowsing to determine the effect of propagation along the British coast. For the major tidal components, current ellipses at the Inner Dowsing are compared with those elsewhere in the area. Some insight into the behaviour of tides in the vicinity of the Wash is obtained by representing each constituent as the sum of a progressive and a standing wave. Finally we present detailed cotidal and coamplitude charts for the principal astronomical constituents O_1, K_1, N_2, M_2 and S_2, in the region.

a) The constancy of the tidal harmonic constituents

Table 2 summarises the amplitudes and phases of the principal harmonic constituents at the Inner Dowsing tower. The values of amplitude and phase obtained by least-squares analysis of a year of data are compared with the values obtained by analysing separately 12 lunar cycles of data for elevation and 11 lunar cycles for currents (one month of current meter data was unsuitable for analysis because of a severely unbalanced meter and fin configuration). For the monthly analyses those constituents which could not be determined individually because of the lower frequency resolution (such as P_1 and K_2) were related by using the values obtained from the analysis of the whole year. The standard deviation of these monthly values about the annual value, and the standard error are also shown, as are the maximum and minimum values obtained during the year. The standard deviations of these 'constants' are significant, because they indicate the confidence which may be placed in values

obtained where observations of off-shore elevations or currents are made for a single lunar month, as is the case with most deployments.

As expected, the larger constituents show the greater stability as they stand out more clearly above the background noise. Conversely, the constituents of the east-west (u) component of current, are less well determined, particularly in the diurnal band where the currents are almost rectilinear in the north-south direction. Some of the variability is due to instrumental limitations, particularly for the currents. At the beginning of the experiment, before crystal clocks had been fitted to the current meters, some phase errors may have been introduced by inadequate corrections for timing errors. Also, for some deployments, the current meter mounting was slightly unbalanced, which resulted in directional errors for the recorded currents.

For the principal semi-diurnal constituent, M_2, the standard error in the elevation amplitude is 0.4%, while for the u and v components of current the errors are 4% and 2.5% respectively.

b) Observed and equilibrium tidal relationships between neighbouring constituents

When analysing short periods of data, for example data extending over a lunar month or less, for harmonic constituents, it is necessary to relate constituents which cannot be individually resolved, using information based on a longer period of data, or on the equilibrium tide. Table 3 summarises the phase and amplitude relationships for some of these paired constituents for the equilibrium tide and for the elevations and currents based on the year's analysis at the Inner Dowsing. The u constituents of current again show greater variability than the v constituents. In general the elevation relationships are close to the equilibrium amplitude ratios; however, they differ enough in phase to be used in preference to the equilibrium relationships for the analysis of short periods of elevation data. The currents show general agreement with both the equilibrium tide and the elevation analysis. In the particular case of the solar semi-diurnal tide S_2 related to the lunar semi-diurnal tide M_2, the elevation and current relationships agree well, but, because of the additional radiational input at S_2, their agreement with the equilibrium tidal relationship is poor. On this evidence, when choosing relationships to apply to a monthly analysis of current meter data, the use of elevation relationships from a year's analysis at a nearby coastal station is recommended.

For shallow-water constituents which have no equivalent in the equilibrium tide, relationships would have to be derived from elevation relationships at a nearby coastal station. The relationships in Table 3 for shallow-water constituents generally show good agreement between elevation and current components, particularly for the phases.

One puzzling feature of the table is the anomalous (0.14) amplitude relationship between K_2 and S_2 in the v component of current compared with the relationships (0.28, 0.26, 0.27) for the elevations, u component of current, and equilibrium tide. This anomaly is also present in the amplitude relationships for the v component of the two shallow-water constituents involving K_2, MKS_2 and MK_4. The phases of these constituents agree well with the elevation relationships.

c) Inner Dowsing tides compared with Lerwick

The astronomical tides propagate southwards into the North Sea, as progressive waves having their maximum amplitude on the British coast due to the Earth's rotation. We have computed the response curves for the tides at the Inner Dowsing tower relative to those at Lerwick, which is at the northern entrance of the North Sea. For Lerwick (Fig. 11) a response analysis, including radiational terms, of six years of data was used to compute hourly heights. The Inner Dowsing elevation data for the period 91/72 to 119/72 was then analysed using the linear predictions at Lerwick as a reference, as proposed by Cartwright, Munk and Zetler [1969]. Shallow water tides at Lerwick are extremely small. The response curves for the semi-diurnal band are shown in Fig. 4. Inner Dowsing elevations are amplified across the band by a maximum of 3.4 around the M_2 frequency. There is a progressively increasing phase lag

with increasing frequency, as would be expected for a nondispersive wave where the time of travel for each wave is independent of frequency; for M_2 this time difference is 7 h 15±1 min. Because of contamination by the shallow-water constituent $2MN_2$, the astronomical term L_2 has a large variability at the Inner Dowsing, and is amplified by a factor of 6.2 compared with Lerwick, indicating the importance of shallow-water tidal generation for water levels at the Inner Dowsing. Similar calculations for the diurnal band give an amplitude response which reaches a maximum of 2.10 around a frequency of 0.96 cpd.

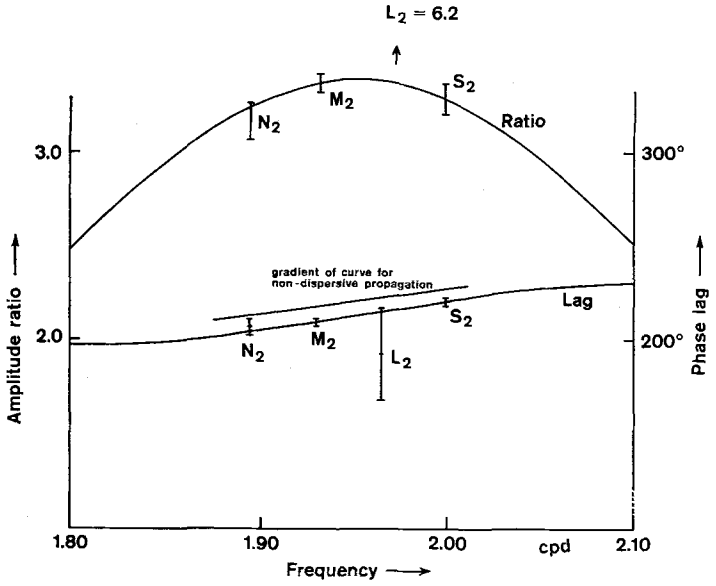

Fig. 4. Semi-diurnal tides: the relationship between amplitudes and phases at the Inner Dowsing and at Lerwick

d) Current ellipses at the Inner Dowsing and elsewhere in the region

Fig. 5 shows the current ellipses plotted from the harmonic analyses of a year of data at the Inner Dowsing, for the six principal tidal bands. The ellipses for the shallow-water tidal bands shown in this figure will be discussed later.

The two long-period tides are the monthly (Mm) and the semi-monthly (Msf). The semi-monthly astronomical term Mf, which is larger than either Mm or Msf in the equilibrium tide, was of comparable amplitude to them in the observed elevations but of considerably smaller amplitude in the observed currents. A comparison of these three constituents is made in Table 4. Msf and Mf may be resolved from each other using six months of data, but the accuracy to which these constituents can be determined is affected by the high noise level at low frequencies. From the spectral analysis of non-tidal residuals we estimate the standard errors in amplitude and phase using the formulae:

$$(\text{standard error})^2 = \tfrac{1}{2}\left(\frac{\text{residual variance}}{\text{signal variance}}\right)\left(\frac{27.3}{\text{time span in days}}\right)$$

where the variance is computed relative to the amplitude itself or to one radian in phase, over a frequency band 1 cpm to 2 cpm.

The standard errors are shown in Table 4. For the plotted current constituents Mm and Msf the estimated standard errors in the east-west and north-south components were 22 % and 28 % respectively, so that the plotted current ellipses are only approximate representations of the long period tidal currents.

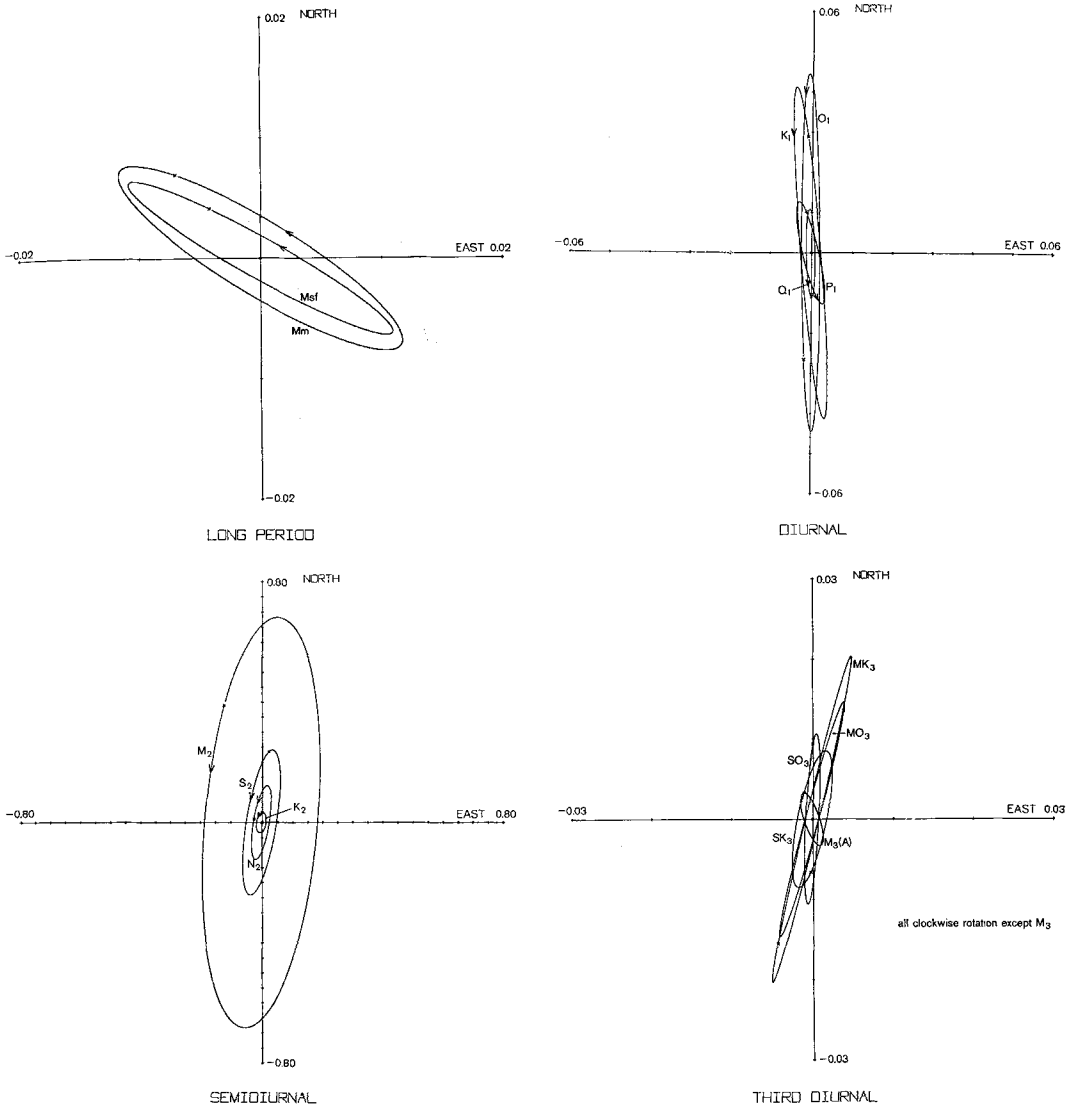

Fig. 5. Current ellipses for the principal constituents in tidal bands at the Inner Dowsing tower. Note the different scales. The arrows show the sense of rotation. Tidal constituents rotate anti-clockwise but shallow-water constituents rotate in a clockwise direction. Speeds in m s^{-1}

The confidence limits for the diurnal and semi-diurnal constituents are best determined from the results of the series of monthly analyses summarised in Table 2. The diurnal band currents which are almost rectilinear in the north-south direction, have small and poorly determined east-west components. Fig. 6 shows the results of a response analysis between the dominant v component of current and the elevations over a period from 91/72 to 119/72. A response analysis is appropriate in determining the relationship between tidal currents and elevations because the transfer admittance is calculated assuming it to be a smooth function of frequency within the tidal band. In both the diurnal and semi-diurnal bands the phase differences and relative amplitudes are very stable. This uniformity of response is confirmed by the similarity of the tidal current ellipses (Fig. 5) for each band. From these ellipses we conclude:

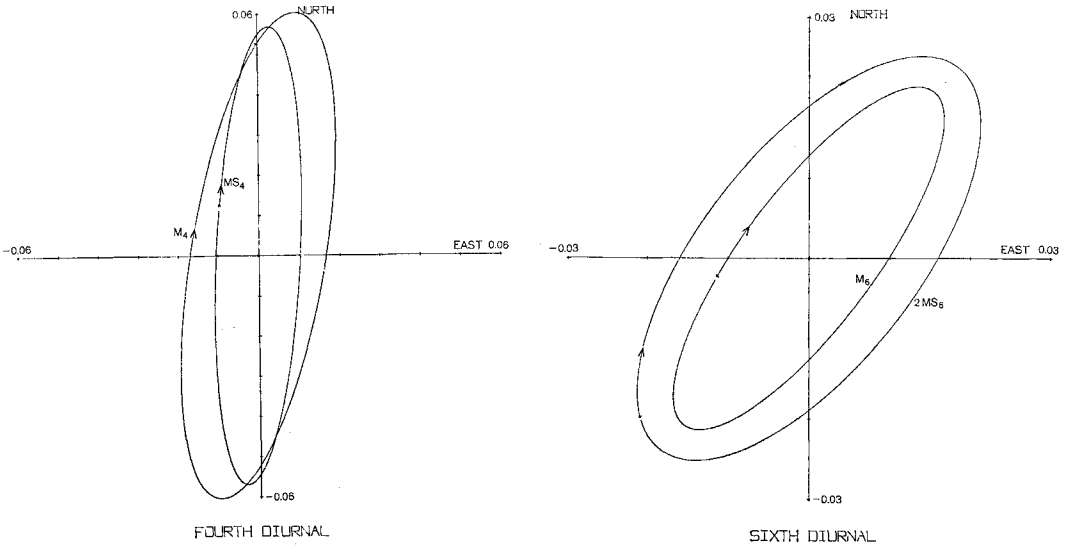

Fig. 5

I) that the sense of rotation of all the plotted constituents in the long period, diurnal and semi-diurnal bands is always anti-clockwise

and

II) that the major axis of the ellipses rotates in a clockwise sense with increasing frequency: the long-period tides are nearly parallel to the British coast, while the semi-diurnal tides are strongly deflected in the direction of the Wash.

The uniform behaviour of tidal current ellipses within a band also applies for observations of only a month of data as is shown in Fig. 7 for the semi-diurnal band at four other current meter stations. At Zo the sense of rotation is anticlockwise, as for the Inner Dowsing, but at the Shell-Esso platform the sense of rotation is clockwise. The ellipses at station A in the Wash are virtually rectilinear (though all rotate in a clockwise sense), while at station B the rotation is anticlockwise.

The sense of rotation of the diurnal current ellipses is variable at Zo and at the Shell-Esso platform, where they are also almost rectilinear. The sense of rotation of a current ellipse vector for a particular constituent is determined by the phase difference between the u and v components. If we represent the components as:

north-south	$V \cos(\sigma t - g_v)$
east-west	$U \cos(\sigma t - g_u)$

then in our convention the direction of flow is:

$$\vartheta = \arctan\left(\frac{V \cos(\sigma t - g_v)}{U \cos(\sigma t - g_u)}\right) \text{ and } \frac{d\vartheta}{dt} \text{ has the sign of } (g_v - g_u)$$

so that $\frac{d\vartheta}{dt}$ is positive (anticlockwise rotation) if

$$0 < g_v - g_u < \pi \text{ or, more generally } n\pi < g_v - g_u < (n+1)\pi \tag{1}$$

for even n and $\frac{d\vartheta}{dt}$ is negative (clockwise rotation) if

$$\pi < g_v - g_u < 2\pi \text{ or, generally } n\pi < g_v - g_u < (n+1)\pi \text{ for odd } n. \tag{2}$$

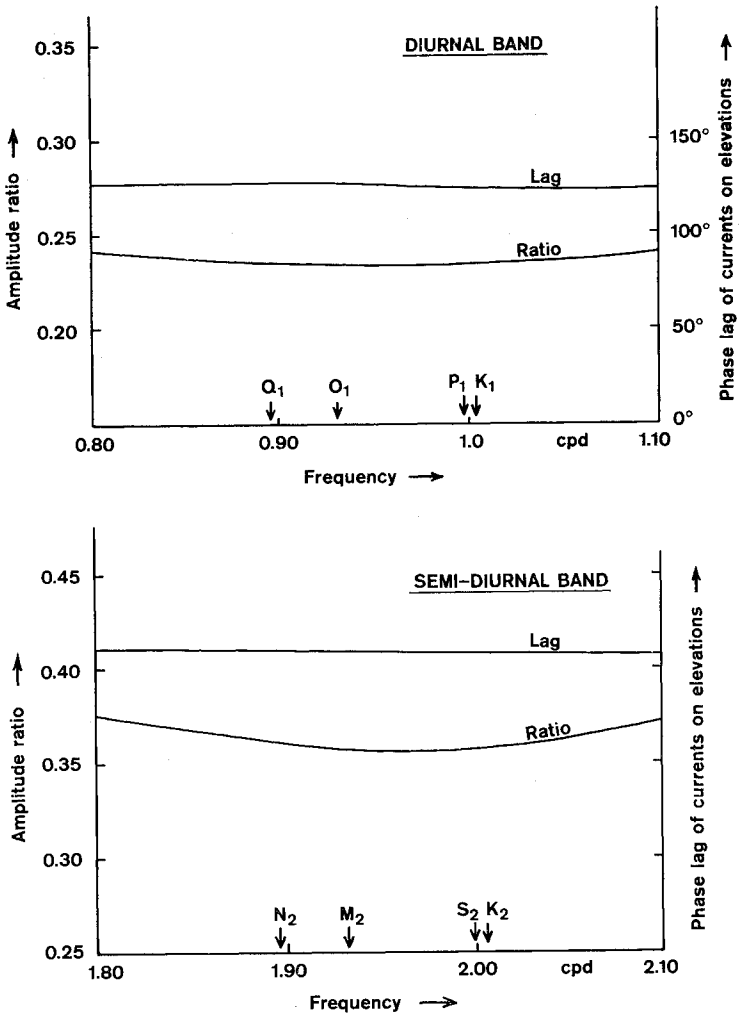

Fig. 6. Phase and amplitude relationships between currents and elevations at the Inner Dowsing tower, in the diurnal and semi-diurnal tidal bands. Currents in m s^{-1}, elevations in m

If $(g_v - g_u) = n\pi$ (n integer) the currents are rectilinear. Using the confidence limits of Table 2 for the O_1 and K_1 constituents at Zo and the Shell Esso platform shows that the different senses of rotation observed are not significant. For example, at the Shell Esso platform:

for O_1 $(g_v - g_u) = -162.5^0 \pm 76.4^0$
K_1 $(g_v - g_u) = \quad 170.0^0 \pm 99.3^0$.

At the two stations within the Wash the sense of the rotation is the same as for the semi-diurnal currents. Table 5 summarises the sense of rotation within the tidal bands.

e) Resolution of tides into a standing and a progressive wave

For a wave propagating parallel to a straight coastline, in the absence of reflected waves, the theoretical solution is a Kelvin wave, where the currents are rectilinear with a maximum in the direction of propagation at the time of local high water. In a bay, such as the Wash, the reflection of the wave at the head produces a standing wave (see Fig. 2 of Alcock and Pugh [1975], for contours of the water surface within the Wash at high water), where the

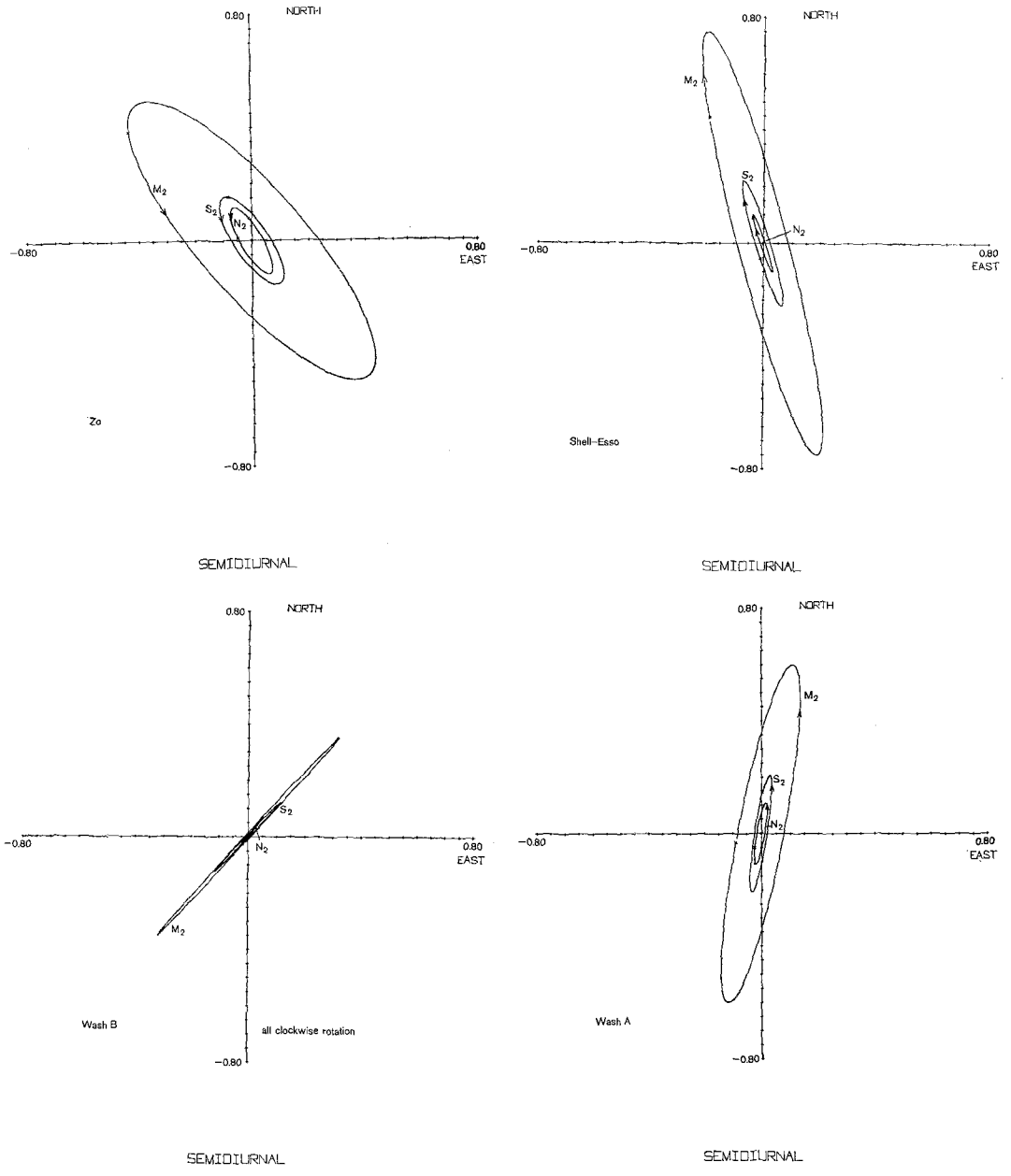

Fig. 7. Semi-diurnal current ellipses for other stations in the region. Speeds in m s^{-1}

currents are a maximum at mid tide. Tidal components for the Inner Dowsing have been resolved into a progressive wave and a standing wave, each having a determined amplitude and direction, to illustrate the influence of the Wash on the observed tides.

Because the region is small compared with a tidal wavelength, the difference in high water times is small compared with a tidal period. Measuring times relative to local high water, consider the currents in a progressive wave at frequency σ to be given by:

$$W_p \cos \sigma t$$

propagating in a direction λ, measured positive anticlockwise from geographic east. The north-south and east-west components are then:

$$\text{n} - \text{s}: W_p \cos \sigma t \sin \lambda, \quad \text{e} - \text{w}: W_p \cos \sigma t \cos \lambda. \tag{3}$$

At $t = 0$ the elevation is a maximum. Similarly, for the standing wave along an axis having direction φ, the currents are given by:

$$W_{st} \sin \sigma t$$

which has components:

$$\text{n} - \text{s}: W_{st} \sin \sigma t \sin \varphi, \quad \text{e} - \text{w}: W_{st} \sin \sigma t \cos \varphi. \tag{4}$$

From our analysis we have the amplitudes (U, V), and phases (δ_u, δ_v), of the north-south and east-west components:

$$\begin{aligned} V \cos (\sigma t - \delta_v) &= V \cos \sigma t \cos \delta_v + V \sin \sigma t \sin \delta_v \\ &\equiv V_1 \cos \sigma t + V_2 \sin \sigma t \end{aligned} \tag{5}$$

$$\begin{aligned} U \cos (\sigma t - \delta_u) &= U \cos \sigma t \cos \delta_u + U \sin \sigma t \sin \delta_u \\ &\equiv U_1 \cos \sigma t + U_2 \sin \sigma t \end{aligned} \tag{6}$$

when δ_v and δ_u are the phases relative to the time of high water in the elevation. Hence, equating the north-south components of (3) and (4) with (5)

$$\left.\begin{aligned} W_p \sin \lambda &= V_1, \\ W_{st} \sin \varphi &= V_2, \\ \text{and similarly for the east-west components from (3) and (4) with (5)} & \\ W_p \cos \lambda &= U_1, \\ W_{st} \cos \varphi &= U_2. \end{aligned}\right\} \tag{7}$$

From which we have the following expressions for the amplitudes and directions of the progressive and standing waves:

$$W_p = \left(V_1^2 + U_1^2\right)^{\frac{1}{2}} \qquad \lambda = \arctan\left(\frac{V_1}{U_1}\right)$$

$$W_{st} = \left(V_2^2 + U_2^2\right)^{\frac{1}{2}} \qquad \varphi = \arctan\left(\frac{V_2}{U_2}\right)$$

φ is the direction of the current in the standing wave on the falling tide.

The amplitudes and directions computed in this way are given in Table 6 for the principal diurnal, semi-diurnal and the long-period tides at the Inner Dowsing, and for the M_2 tide elsewhere. We return to considerations of energy fluxes later, but note here that the direction of flux is the direction of progressive wave propagation, and that the magnitude of the flux is almost proportional to the square of the progressive wave amplitude. At the Inner Dowsing all the progressive waves advance in a southerly direction with the long-period tides directed furthest towards the east. The standing wave is directed along an axis towards the Wash for the diurnal and semi-diurnal tides. The anticlockwise direction of rotation of the current ellipses is due to the standing wave ebb flow from the Wash following the south going flow of the progressive tide at high water. For the long-period tides the standing wave direction is along an east-west axis towards the Lincolnshire coast. For these long period tides, which have a wavelength of several thousand kilometers the dimensions of the Wash are too small to have much influence on the wave propagation which is more likely to be influenced by the dimensions of the North Sea as a whole.

Within the Wash, for the M_2 tide, the progressive wave is very small and the standing wave is dominant. At Zo there is a small standing wave component, but the progressive wave is dominant. At the Inner Dowsing and at Zo the flow is away from the coast on the falling tide. However, at the Shell-Esso platform, which is in a complex region of parallel shallow banks (Fig. 1), there is a large standing wave, with a flow towards the coast on the falling tide although the progressive wave is still directed in a southerly direction parallel to the coast. These calculations are summarised in Fig. 8.

f) Cotidal and coamplitude charts for the region

Fig. 9 (a to h) shows the results of combining all of the elevation and current observations to produce cotidal and coamplitude charts for the region. Phases are in degrees relative to the equilibrium tide at Greenwich and amplitudes are in metres. The current meter observations were combined with elevations, as described by Proudman and Doodson [1924] in their

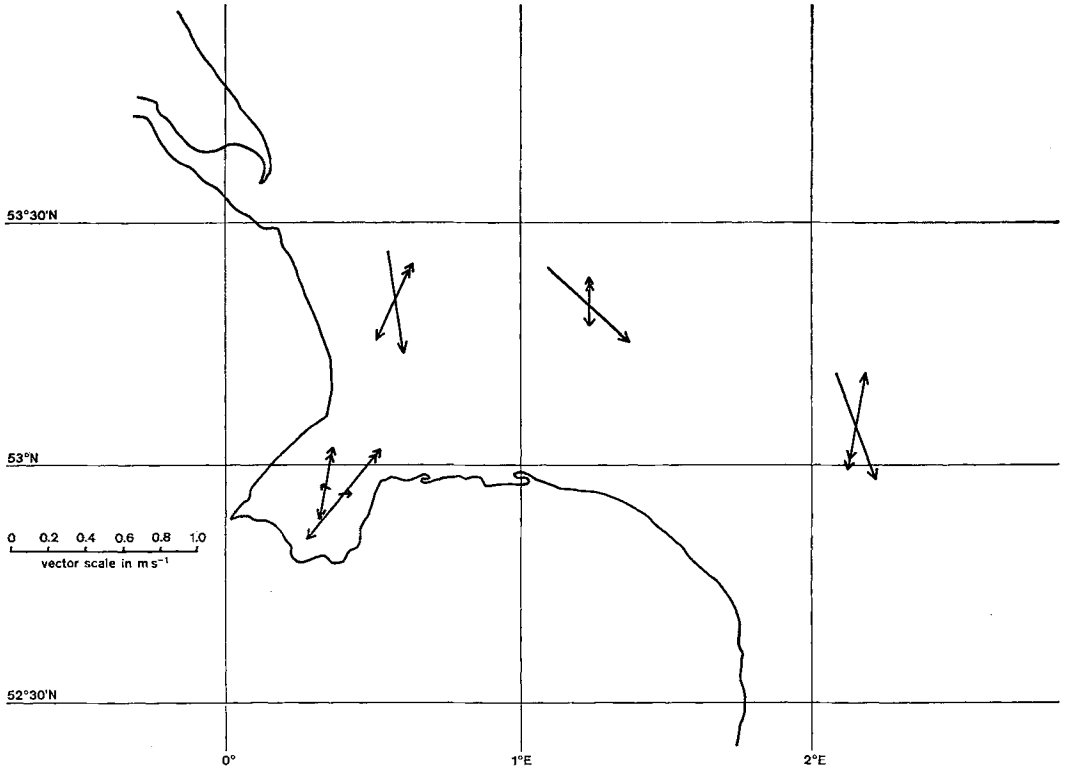

Fig. 8. Plots of progressive and standing wave configurations in the Dowsing region of the North Sea. Progressive waves have a single arrow. The double arrow gives the direction of standing wave flow on the falling tide

classical account of the behaviour of the M_2 tide in the North Sea, to give both the directions and the gradients of the cotidal and coamplitude contours. Frictional terms at each frequency were computed by first applying a quadratic law to obtain the instantaneous components of friction every hour, and then analysing a lunar month of these components for the harmonic components at the tidal frequencies. The final plotting of the lines was done by hand. Although, inevitably, this is a subjective process, their validity may be considered in terms of the maximum differences between the smoothed curves and the observations on which they were based.

In the diurnal band, the maximum discrepancy for O_1 occurs at the North Star rig, where the chart amplitude is 0.02 m lower than that observed, and the chart phase is 15^0 lower than observed. At Gibraltar Point the chart phase is 2^0 low. For K_1 the chart phase at the Shell-Esso platform is 2^0 low and at Skegness, 4^0 low. The observations at Gibraltar Point give anomalous values for K_1 (the observed amplitude is 0.03 m too high and the phase 14^0 too high); this is probably due to the method of observation – reading tide poles over a period of a month – where systematic differences between daylight and darkness readings are likely.

In the semi-diurnal band the observed N_2 phase at Roaring Middle is 4^0 lower than that shown on the chart, while the observed amplitude at West Stones is 0.03 m lower than indicated.

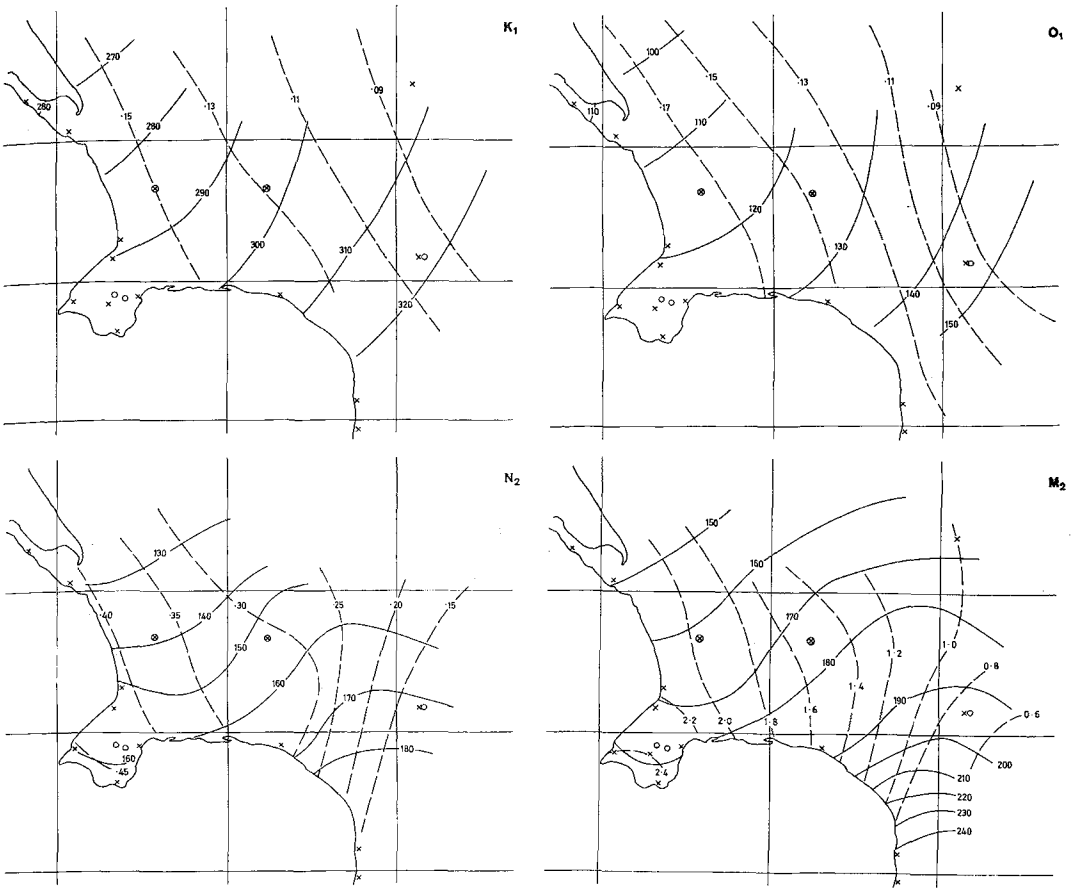

Fig. 9. Cotidal and coamplitude charts for the Dowsing region of the North Sea. Phases are in degrees relative to the equilibrium tide at Greenwich; amplitudes in metres. Elevation observations (x). Current observations (o)

For M_2 the maximum discrepancies occur at Tabs Head and West Stones, where the observed amplitudes are 0.03 m and 0.10 m lower than those indicated on the charts, due to the influence of river discharge on low water levels. For the M_2 chart, observations based on a month of data were corrected to give an approximate mean annual value by normalising them with respect to the analysis of simultaneous Inner Dowsing data, in an attempt to allow for the annual modulation discussed earlier. For S_2 the maximum discrepancy again occurs in the Wash, where the observed phase at Roaring Middle is 3^0 lower than that shown on the chart and the observed amplitude at West Stones is 0.05 m lower than shown. At the Inner Dowsing the observed amplitude is 0.02 m higher than shown on the chart.

The two principal charts with which these may be compared are the Proudman and Doodson chart of the M_2 constituent in the North Sea, and the German tidal charts (Oberkommando der Kriegsmarine [1942]) for ten major constituents. All charts of M_2 have a progression of the tide southwards along the British coast. All three charts agree well for both phase and amplitude near the Inner Dowsing, but the present chart is more detailed, particularly within the Wash. The greatest discrepancies occur in the directions of the cotidal lines near the Shell-Esso platform. Our results show a cotidal line directed at -24^0 (measured anticlockwise from east), while on the Proudman and Doodson chart the direction is due east and on the German chart, 045^0. The amplitudes and phases are respectively: (0.74 m, 195^0),

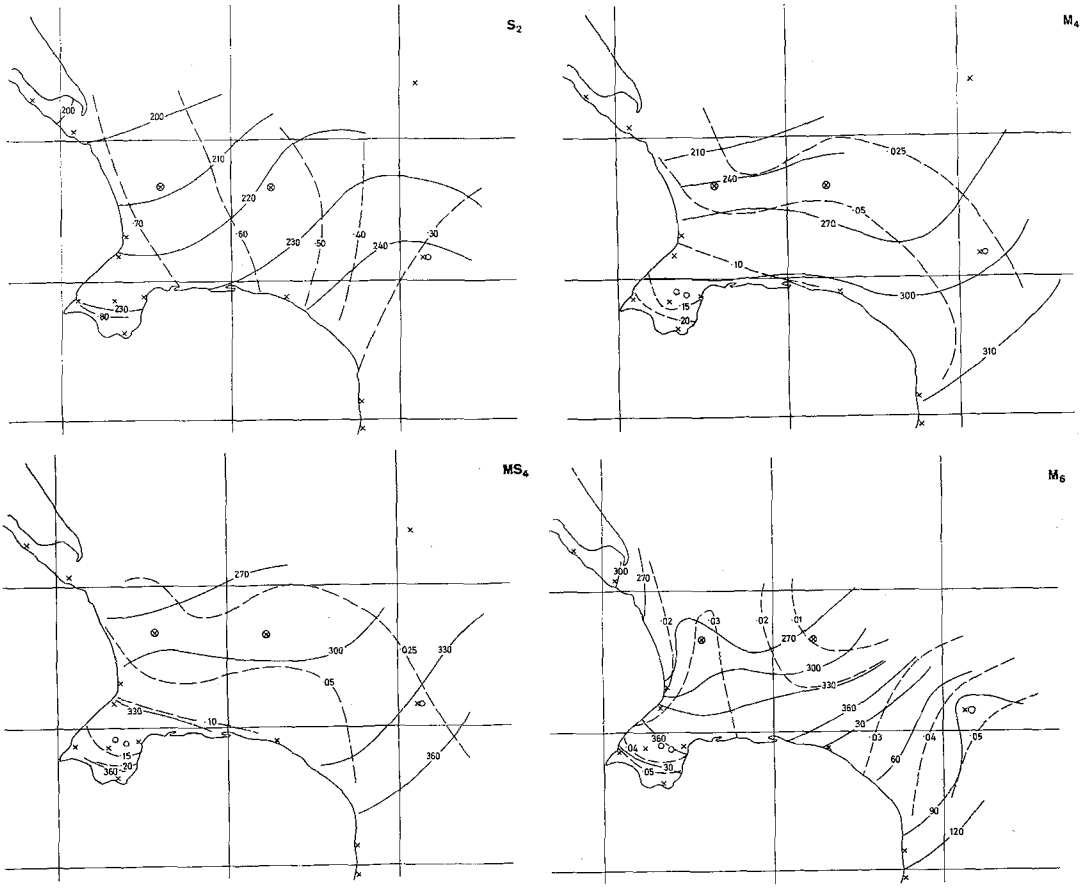

Fig. 9

(0.90 m, 205°) and (0.75 m, 215°). The errors in the earlier charts arise from problems in locating the amphidrome in the southern North Sea, using very little off-shore data.

Not surprisingly the other two constituents in the semi-diurnal band both have similar characteristics, and differ most markedly from the German charts around the Shell-Esso platform. The overall picture is of a progressive wave propagating south along the coast, with cotidal and coamplitude lines orthogonal. Within the Wash the lines become parallel, characteristic of a standing wave. In the east the picture is more complicated as the cotidal lines converge towards the amphidrome.

The major difference between the German charts for O_1 and K_1 and those presented here is in the amplitudes; our amplitudes are some 50 % larger. Also, our cotidal lines are closer together, indicating slower progression through the region. For these diurnal constituents the influence of the Wash is less apparent, and there is no trend towards an amphidrome in the southern North Sea.

The shallow water tides

The results for shallow-water tides are shown in Fig. 5 and 9, and in Table 5. At the Inner Dowsing tower the shallow-water tides are relatively more important in the currents than they are in the elevations. For example, in elevations the M_4 amplitude is 1.8 % of the M_2 amplitude, while for the north-south component of current the ratio is 8.9 % and for the east-west component 10.0 %.

a) Current ellipses at the Inner Dowsing and elsewhere in the region

Fig. 5 shows that for the shallow-water tidal bands the current ellipses are stable within a band, as for the astronomical tides. For the third-diurnal and fourth-diurnal bands the major axis lies almost north-south, as for the diurnal and semi-diurnal bands. However, the most striking property of all these ellipses is that they all rotate in the opposite sense to the astronomical current ellipses, that is clockwise. The only exception is the very small constituent M_3, which rotates anticlockwise, as do the astronomical current ellipses but of course M_3 is of astronomical origin. The relationship between the sense of rotation of the astronomical components and the shallow-water components elsewhere in the region is summarised in Table 5. At each position the current ellipses in the third and fourth diurnal band rotate in the same sense as each other and, apart from Station A in the Wash, this direction is always in the opposite sense to the rotation of the semi-diurnal current ellipses. The behaviour of the ellipses in the sixth-diurnal band is less regular.

b) Shallow-water cotidal and coamplitude charts

One of the major problems associated with an understanding of shallow-water tides is a knowledge of the extent of their spatial coherence. Fig. 9 (f and g) show the charts for M_4 and MS_4, constructed from the elevation and current data as was done for the astronomical terms. In both charts the patterns are remarkably similar and can be followed coherently across the region. As for the astronomical tides the progression is from north to south, with the cotidal and coamplitude lines approximately orthogonal away from the Wash. Within the Wash itself the amplitudes increase rapidly towards the head of the bay. Although the cotidal and coamplitude lines are parallel, as for a standing wave, the amplification which occurs is far greater than would be expected for a standing wave, showing that there is local generation of the constituents. Resolving into progressive and standing waves, at the Inner Dowsing the M_4 direction of propagation, measured positively anticlockwise from east, is 71^0, that is, away from the Wash. At Zo it is -50^0 and at the Shell-Esso platform it is -23^0, that is, the direction of propagation is south, approximately parallel to the coast. The charts have not been extended far to the north of the Inner Dowsing tower because rapid phase changes occur between the tower and the Bull Sands Fort observations, which would be difficult to represent accurately with the limited data available. The German charts of M_4 and MS_4 for the region bear little resemblance to those presented here.

Fig. 9 (h) shows the chart for the M_6 constituent. Although the amplitudes are only a few centimetres, it was still possible to draw a chart. The major difficulty was in reconciling the calculated gradients for the cotidal lines at the Inner Dowsing tower and the Shell-Esso platform with the general regional pattern. Because the calculated gradients were very small, this resulted in large excursions for the 270^0 and 90^0 phase lines. Again the overall pattern is one of wave progression from north to south through the region, but in this case the amplitude of the wave increases as it progresses towards the south-east past the Shell-Esso platform, in contrast to the fourth-diurnal terms, where the amplitude increases towards the coast.

The Proudman and Doodson method of computing gradients of cotidal and coamplitude lines assumes free waves (no local forcing). The difficulty in reconciling the calculated gradients in the cotidal lines for M_6 with the regional pattern is probably due to the waves being locally generated. The better agreement of the M_4 and MS_4 gradients suggests that local generation has less effect, except in the Wash where their amplitude increases rapidly.

Shallow-water tides, arising as they do from non-linear processes, are very difficult to treat theoretically, particularly in two dimensions. Numerical computation in the Wash (Alcock and Pugh [1975]) have shown how the advective terms in the hydrodynamic equation produce a fourth-diurnal elevation component at Hunstanton relative to Roaring Middle, in an area where the curvature of the streamlines is high. Generally, this advective effect may be less important than the effects of bottom friction and changes in depth during the tidal cycle. It is suggested that the north to south progression pattern for all three plotted shallow-water constituents, at velocities approximately the same as for the astronomical tides, is due

less to their being external waves propagating through the region, than to their phases being controlled during local generation by the phases of the astronomical tides.

c) The effects of asymmetrical flow on analyses of shallow-water tides

One possible explanation of the opposite sense of rotation of the astronomical and shallow-water current vectors is the asymmetry of the north-going and south-going flows. Fig. 10

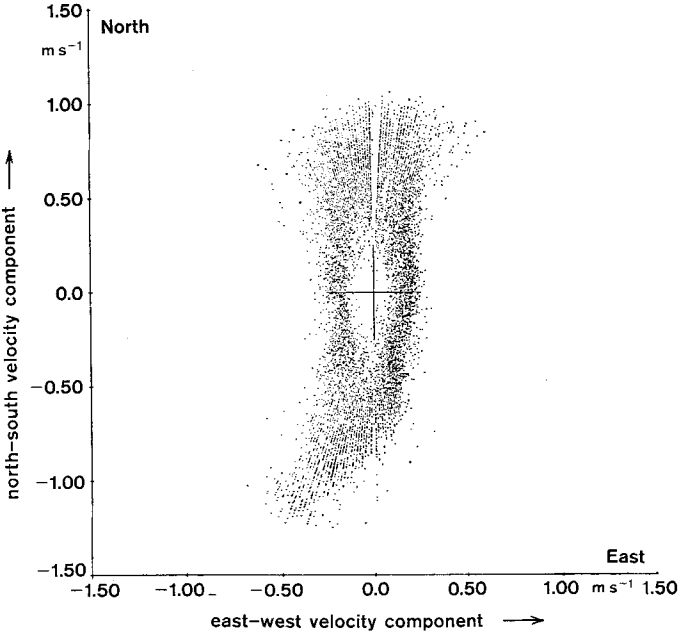

Fig. 10. Vector dot diagram of recorded 10 minute currents at the Inner Dowsing tower, day 84/72 to 138/72. Note the non-rectilinear flow pattern for large speeds

shows the distribution of 10 minute current vectors over a typical period of 54 days. The mean north-going flow is directed almost due north, but the south-going flow is deflected westwards towards the Wash, particularly for very strong currents.

This deflection for strong currents is probably due to the increased area of water in the Wash on spring tides, which requires a greater water input for a unit increase in sea level.

Consider a current ϱ along some axis, which may be written:

$$\varrho = W_+ \sin \sigma t \quad \text{for negative } \sin \sigma t \text{ i.e.} -\pi < \sigma t < 0$$
$$\varrho = W_- \sin \sigma t \quad \text{for positive } \sin \sigma t \qquad 0 < \sigma t < \pi$$

expanding this as a Fourier series:

$$\varrho(\sigma t) = \frac{(W_+ - W_-)}{\pi} + \frac{(W_+ + W_-)}{2} \sin \sigma t - \frac{2}{3\pi} (W_+ - W_-) \cos 2\sigma t - \frac{2}{15\pi} (W_+ - W_-) \cos 4\sigma t. \tag{8}$$

Writing this in terms of cosines with positive coefficients, and neglecting the terms above cos $(2\sigma t)$

$$\varrho\left(\sigma t + \frac{\pi}{2}\right) = \frac{(W_+ - W_-)}{\pi} + \frac{(W_+ + W_-)}{2} \cos \sigma t + \frac{2}{3\pi} (W_+ - W_-) \cos 2\sigma t. \tag{9}$$

If the first harmonic term is written in the usual tidal notation:

$$W_1 \cos(\sigma t - g_{w_1}) \tag{10}$$

we have

$$\varrho\left(\sigma t + \frac{\pi}{2} - g_{w_1}\right) = \frac{(W_+ - W_-)}{\pi} + \frac{(W_+ + W_-)}{2}\cos(\sigma t - g_{w_1}) + \frac{2}{3\pi}(W_+ - W_-)\cos(2\sigma t - 2g_{w_1})$$

so that a tidal constituent in the fourth-diurnal band has been produced by the asymmetrical flow.

Suppose we have our two orthogonal components:

$$\frac{(U_+ - U_-)}{\pi} + \frac{(U_+ + U_-)}{2}\cos(\sigma t - g_u) + \frac{2}{3\pi}(U_+ - U_-)\cos(2\sigma t - 2g_u),$$

$$\frac{(V_+ - V_-)}{\pi} + \frac{(V_+ + V_-)}{2}\cos(\sigma t - g_v) + \frac{2}{3\pi}(V_+ - V_-)\cos(2\sigma t - 2g_v).$$

The sense of rotation of the principal harmonic component is given by either equation (1) or (2) depending on:

$$(g_v - g_u)$$

and of the second harmonic component, since the amplitude coefficients must be positive:

$$2(g_v - g_u) + \pi \text{ (if } V_- > V_+) - \pi \text{ (if } U_- > U_+). \tag{11}$$

For the M_2 component at the Inner Dowsing:

$$(g_v - g_u) = 73.6^0$$

and so the sense of rotation of the current ellipse is anticlockwise from (1). From the Inner Dowsing data:

$$V_- < V_+$$
$$U_- > U_+$$

so (11) becomes

$$2 \times 73.6^0 - \pi = -32.8^0.$$

Hence from (2) the rotation is clockwise. The opposite sense of rotation of the M_4 current vector to the M_2 current vector may be explained in terms of the asymmetrical flow. From the analyses of the observations the phase difference $(g_v - g_u)$ for M_4 was -60.4^0, giving good agreement, but also showing that the shallow-water terms in the currents are not due to asymmetric flow alone.

For the Inner Dowsing current measurements it is not possible to say to what extent the asymmetrical flow is due to the configuration of the tower, and how much is a genuine oceanographic effect. However, such asymmetry is not uncommon. Admiralty chart 1190, which covers the area from Flamborough Head to Blakeney (53°N, 1°E), gives details of tidal currents at 18 stations, three of which have an asymmetry of more than 20° between principal directions of the flood and ebb flows. Analysis of current data from these stations would also give enhanced fourth-diurnal constituents.

d) The annual modulation of the M_2 constituent

Because the monthly amplitudes and phases of the M_2 elevations showed a systematic variation throughout the year it was decided to investigate this effect in more detail. An annual modulation of the M_2 constituent of elevation has been discussed by Corkan [1934] in terms of two additional constituents which we denote by H_1 and H_2:

H_1	28.94304°/h
M_2	28.98410°/h
H_2	29.02517°/h.

These constituents are separated from the M_2 constituent by one cycle per year, and so may be independently determined in the analysis of a year of data. In monthly analyses, however, they interfere with M_2 giving an apparent modulation. Our year's analysis of Inner Dowsing elevations included these constituents, using nodal corrections f and u as for M_2, and also:

$$V(H_1) = V(M_2) - h$$
$$V(H_2) = V(M_2) + h$$

where h is the mean longitude of the sun. Similar analyses were made of one year of data (1972) from the ten other tide gauges shown in Fig. 11. Fig. 12 shows the phase progression

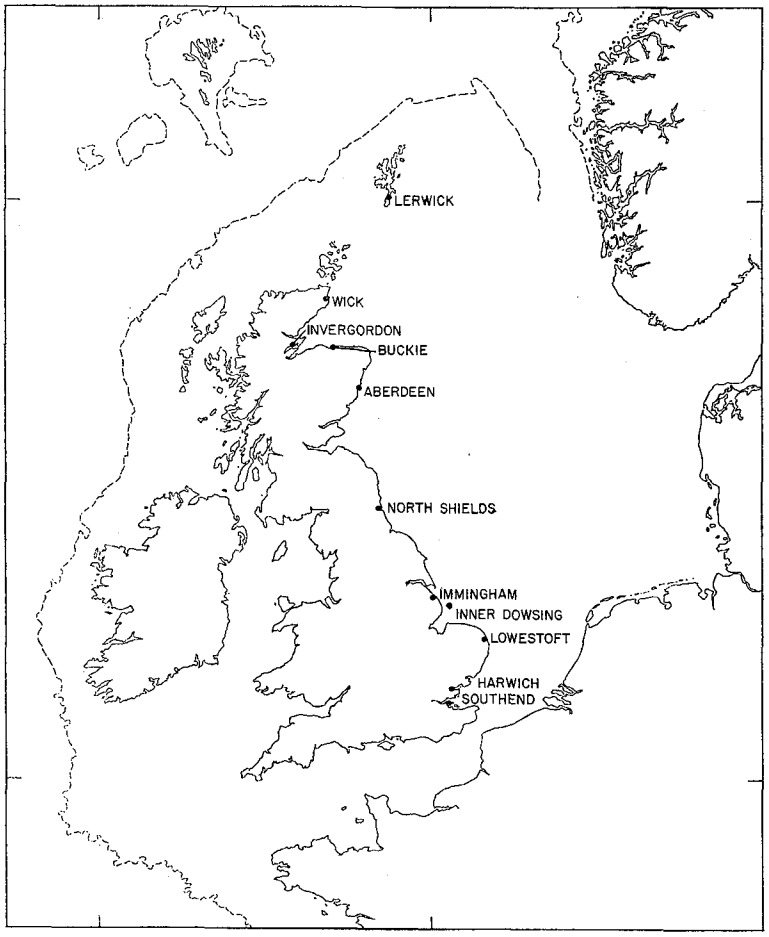

Fig. 11. North Sea ports used for the analysis of water level data to determine the constituents which give an annual modulation to M_2

and amplitude ratios for the H_1 and H_2 constituents as a function of distance measured from north to south along the British coast. As is well known, the M_2 wave propagates south along the coast. For both the H_1 and H_2 constituents the speed and direction of propagation are the same as for M_2. The amplitudes of H_1 and H_2 average at approximately 1 % of M_2, but locally H_1 is greater than 2 % of M_2 at Aberdeen, Immingham, Harwich and Southend. The relative amplitude of both constituents is small at Lerwick.

The cause of these modulations, which have phase coherency along the length of the British coast, is not easily identified. Any harmonic constituent may be represented by the

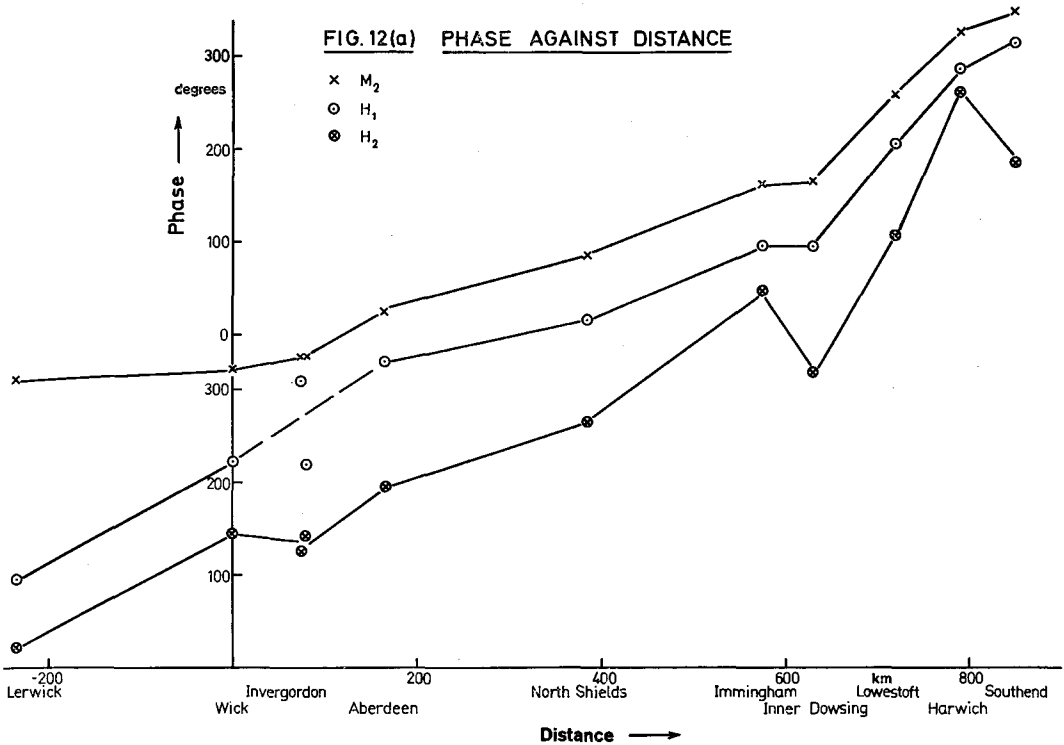

Fig. 12a. The annual modulation of M_2 along the east coast of Britain showing the phase progression of the modulating constituents H_1 and H_2

vector sum of a number of components having the same angular speed but with different amplitudes and phases, so the H_1 and H_2 constituents may be considered to have more than one cause. One specific cause is the astronomical forcing at these angular speeds. In shallow water another cause is the influence of the change in depths on the speed of propagation of the M_2 wave. The former effect is global whereas the latter, which will affect the phase of M_2, will only be important in regions where the water is shallow and the annual variation in water level (Sa) is relatively large. Consideration of these two factors shows that both make only small contributions.

Astronomical forcing functions do exist at the speeds of H_1 and H_2. It is reasonable to suppose the response of the oceans to these astronomical forcing functions will be the same as for M_2 since the angular speeds are so close. Table 7 shows the expected amplitudes and phases for the astronomical H_1 and H_2 input, at each port, using the tide generating potential as developed by Cartwright and Tayler [1971], and compares them with the amplitudes and phases from the analyses of the observations. The final columns show the amplitudes and phases for the non-astronomical H_1 and H_2 components obtained by subtracting the astronomical constituents from the observed constituents. These non-astronomical components are much larger than the astronomical constituents.

Where the tide propagates in shallow water with a velocity $(gd)^{\frac{1}{2}}$ where g is gravitational acceleration and d is mean water depth, any change in d will change the phase of the tide. The annual variation of mean sea level in the North Sea (Sa) should give an annual phase modulation of the tide, particularly in the south where the time of travel through the shallow water is larger. However, taking the value of Sa at North Shields as an average for the North Sea, in November (annual mean sea level + 0.06 m) the tide would be 0.8 minutes earlier than

average, and in May (annual mean sea level −0.06 m) the tide would be 0.8 minutes later than average. Thus, changes in water depth can account for only a small part of the time variation, even at Southend.

Since neither of the above effects can produce the observed modulation, are the causes local, within the North Sea, or are they generated externally? The amplitudes of H_1 and H_2, relative to M_2, fluctuate as the wave travels from Wick to Southend. The local conditions at

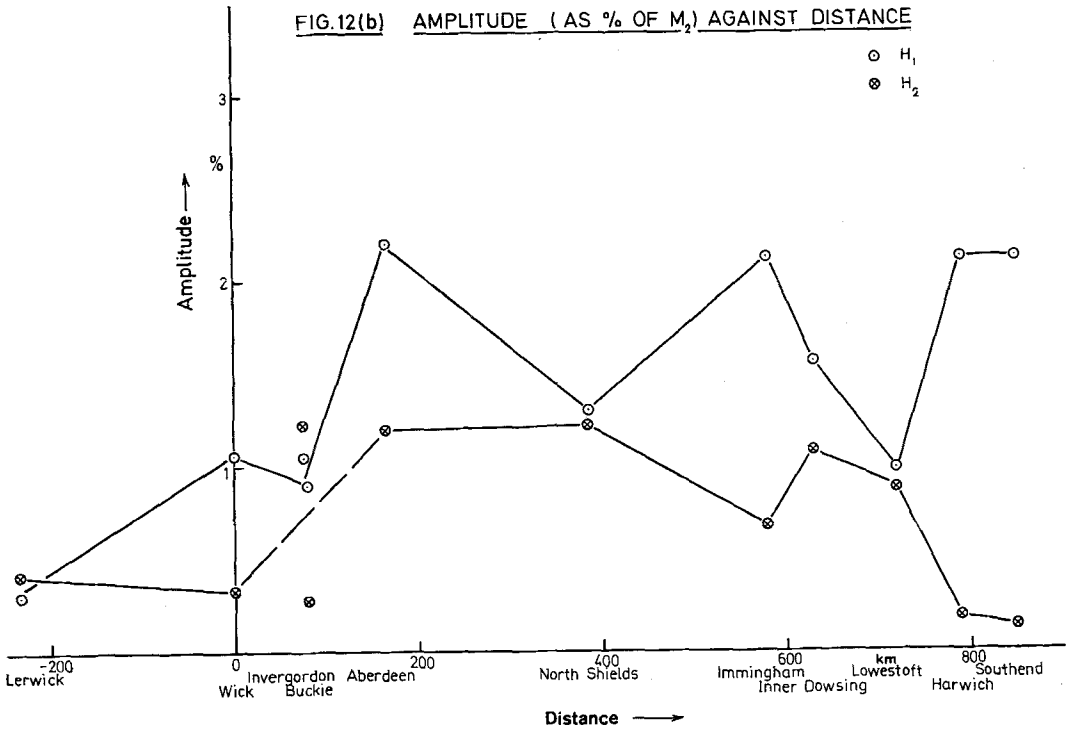

Fig. 12b. The annual modulation of M_2 along the east coast of Britain showing the amplitude ratio of H_1 and H_2 relative to M_2

each port may make different contributions to the perturbation of the tide. The variation is more evident in the amplitudes than the phases and, in both cases some of the scatter must be due to the effect of noise on the analyses. The phase progression along the British coast could be due to two external waves travelling as M_2 travels, but could also be due to the modulation being related to the phase of the dominant M_2 term by non-linear interaction. The evidence from the current meter measurements is not very reliable as the modulations are too small to be accurately measured, but the current ellipses and directions of progressive wave propagation do not fit the normal pattern for the semi-diurnal band, suggesting local effects are present.

Further investigations would require similar analyses for other ports around the British Isles and elsewhere in order to compare further the spatial coherency of these constituents, and analyses of several years of elevation data from a few ports to determine the stability of the constituents from year to year. Cartwright [1968] considers the annual amplitude and phase modulations of M_2 at a number of ports around north and east Britain, and finds that the maximum amplitudes generally occur during the months March to June, while maximum phases occur in January to February. This general pattern also applies for the modulations reported here. Examples of the effects of the constituents on 1972 tidal times and ranges are given in Table 8.

Non tidal residuals

There are two commonly used methods for computing the non-tidal residuals in a time series of water levels or currents. Either the tidal value is predicted using constants derived by a tidal analysis of the data, and then subtracted from the observed value to give a residual:

residual = observed value − predicted value

or the data is subjected to a filter which suppresses energy in the tidal bands, leaving the energy in the non-tidal parts of the frequency spectrum as the residual. The latter method is often used in the form of a low-pass filter where all energy at diurnal and higher frequencies is eliminated. The most important distinction between the two techniques is that the residuals computed from tidal predictions contain energy in the tidal bands, because energy which is not tidally coherent is not included in the tidal predictions. With a filter, both coherent and non-coherent energy is suppressed.

The characteristics of the three low-pass filters used in this work are shown in Fig. 13. The Doodson X_0 filter has the advantage of a short half length but its cut-off is not sharp.

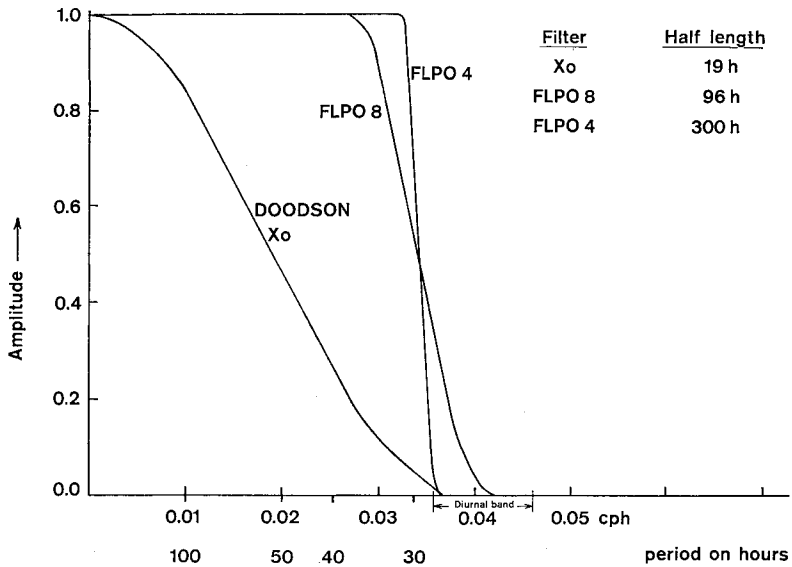

Fig. 13. Frequency characteristics and half-lengths of the low-pass filters used in this paper

The filters FLPO4 and FLPO8, which have half lengths of 300 hours and 96 hours respectively, lose more data because of their half-lengths but have sharper cut-offs. The FLPO8 filter was designed to filter the current meter data, which were in blocks of less than 60 days, without a substantial loss of data, and with a sharp cut-off below a period of 30 hours. The tail of this filter enters the diurnal band, but, even at O_1, the attenuation factor is 92%.

Fig. 14 shows the results of applying the X_0 filter to elevations and currents at the Inner Dowsing from 91/72 to 120/72. All three time series show quasi-periodic oscillations with a period around 3 days – each series has ten maxima in the 30 day period. These oscillations were characteristic of the residuals over the year of observations. There is an obvious negative correlation between the elevations and the north-south component of current due to the southward progression of the surges. Previously, Darbyshire and Darbyshire [1956] have analysed coastal water level data from the winter of 1953–4 and found evidence of energy between 40 and 50 hour period. Because we have available a year of simultaneous elevation and current measurements, a detailed examination of the residual spectrum is worthwhile.

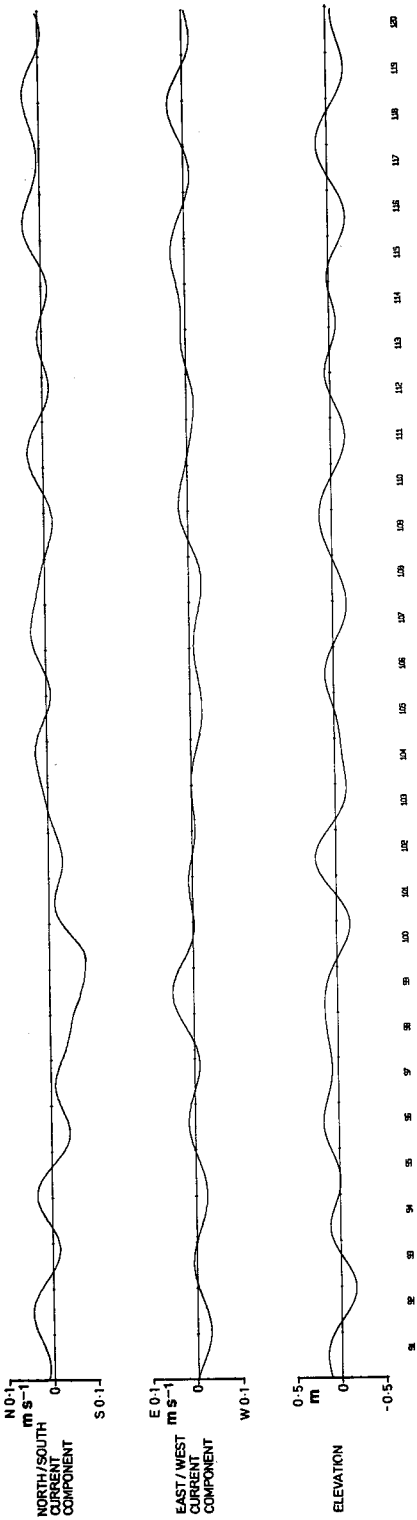

Fig. 14. Low-pass filtered elevations and currents at the Inner Dowsing tower showing non-tidal activity of approximately 3 day period. The negative correlation between elevations and the north-south current component indicates a southerly surge progression

a) Spectral analysis of elevation and current residuals at the Inner Dowsing

Residuals for the year of elevation and current data were computed by subtracting the predicted tidal values (using 102 harmonic constituents) from the observed values. The results of spectral analyses of these residuals are shown in Fig. 15. Fig. 15a (1, 2, 3) give the results

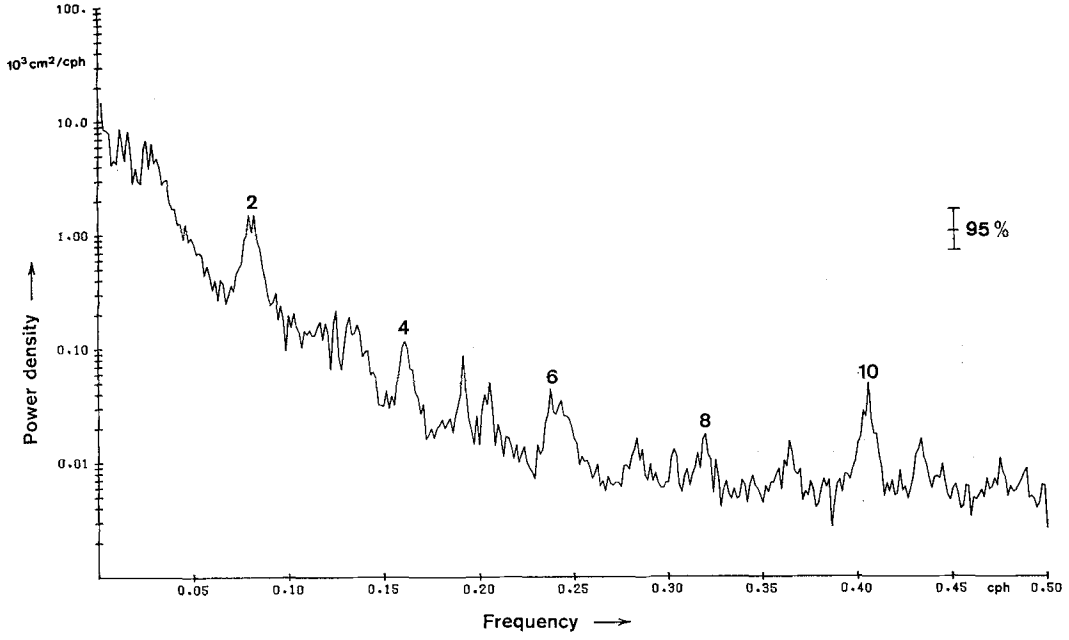

Fig. 15a (1)

Fig. 15. Power density spectra for residual water levels and currents at the Inner Dowsing for the year 064/72 to 063/73, and for the month 277/72 to 304/72 for comparison. Superior numbers show the tidal band locations

of analysis of a year. Comparison with Fig. 15b (1, 2, 3), which show the results of the analysis of a month of data illustrates the superiority of analysing the year of data, as the noise levels are substantially reduced. 95% confidence limits are shown on each diagram.

The distribution of energy at non-tidal frequencies shows significant differences among the three plots. For the elevations the energy falls with increasing frequency and then remains approximately constant above 0.25 cycles per hour (cph). The weak u component of current at non-tidal frequencies has a fairly constant level below 0.25 cph then falls away, while the v component falls steadily with increasing frequency throughout the range. The levels of the residual energy in both currents components are similar except at frequencies around 0.15 to 0.25 cph, where the u component has the greater residual energy.

Within the tidal bands this enhancement of residual energy in the u component of current is also apparent in the fourth-diurnal where it is comparable in amplitude with the residual energy in the semi-diurnal band. This may be an instrumental effect, because the u component is substantially weaker than the v component. The Aanderaa current meters integrated the speed (ϱ) over a 10-minute period, but made only instantaneous readings of direction. Because the instantaneous direction may differ from the direction of the mean flow during the integrating period by an angle $\Delta\vartheta$, the direction record is inherently noisier. This error is distributed unevenly between the direction of mean flow and the orthogonal direction in the ratio:

$$\varrho(1-\cos\Delta\vartheta):\varrho\sin\Delta\vartheta$$

or $\varrho\frac{\Delta\vartheta^2}{2}:\varrho\Delta\vartheta$ for small $\Delta\vartheta$. Since, for these measurements, ϱ was a maximum in an ap-

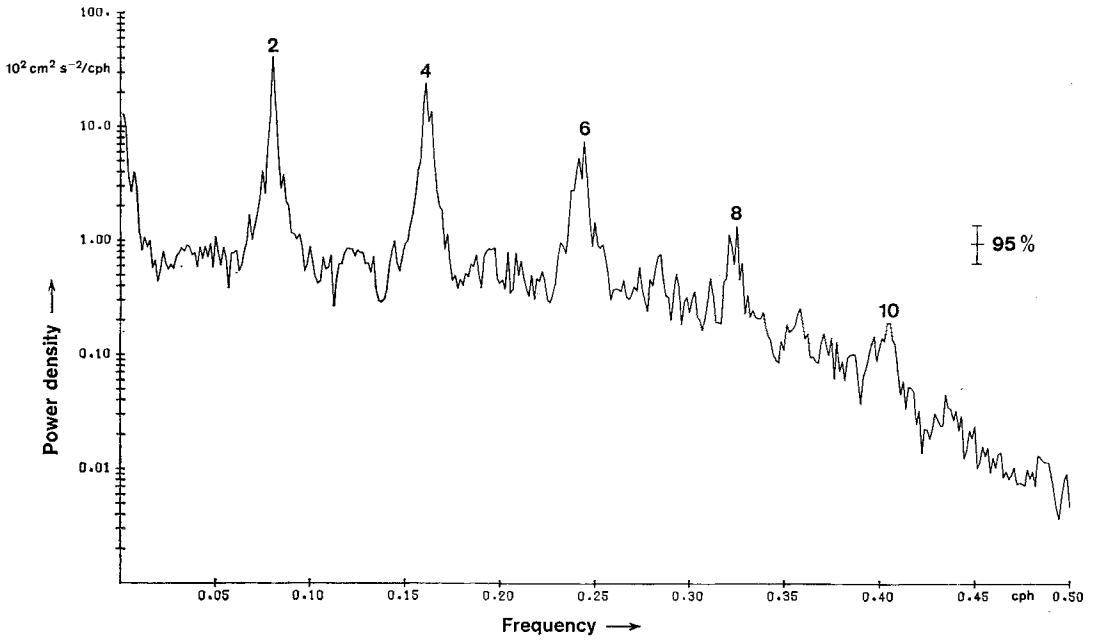

Fig. 15a (2)

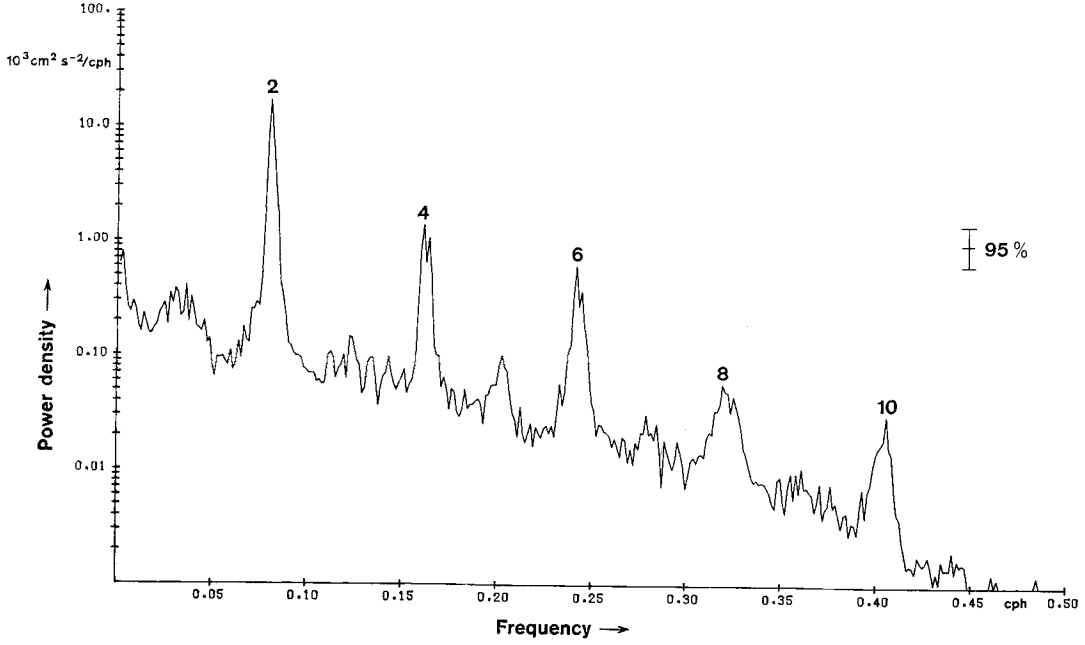

Fig. 15a (3)

proximately north-south direction, most of the noise appeared in the east-west (u) component. Further, since the current speed is a maximum twice during a semi-diurnal period there was an enhancement of residual energy around the fourth-diurnal band. A second instrumental effect is due to the unidirectional properties of the Savonius rotor of the Aanderaa current

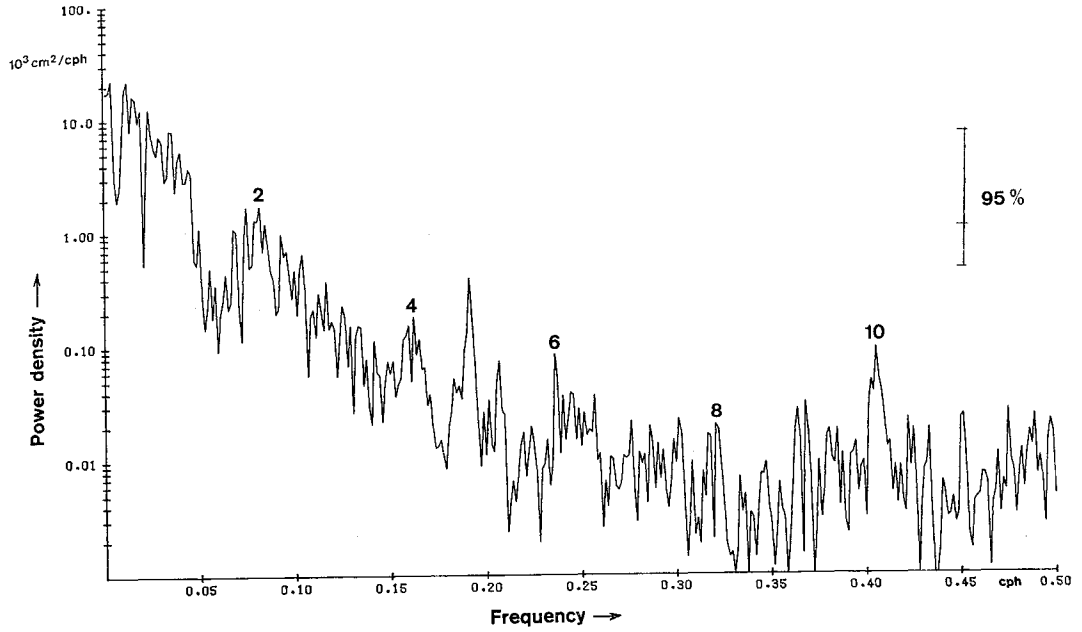

Fig. 15b (1)

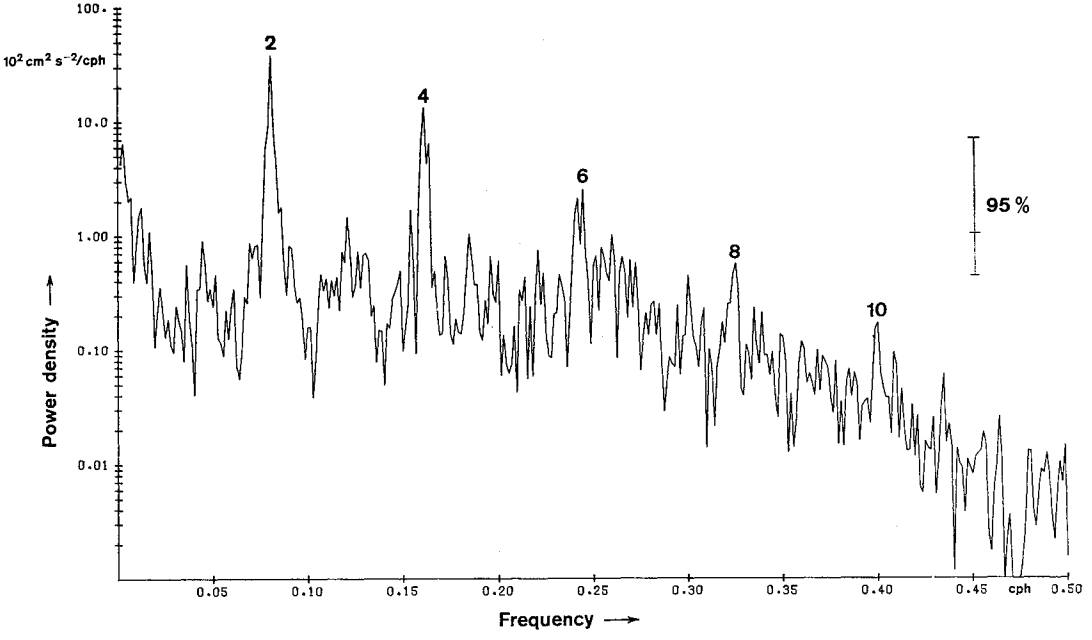

Fig. 15b (2)

meter (Ramster and Howarth [1975] discussions, part b), whereby the rotor records higher speeds than actually occur for tidal streams that are lower than the orbital velocity of the waves. The weaker u component would be more vulnerable to this kind of error.

For both current components the residual energy in the even tidal bands stands out from the background energy up to the tenth-diurnal band. However, only in the fifth-diurnal band

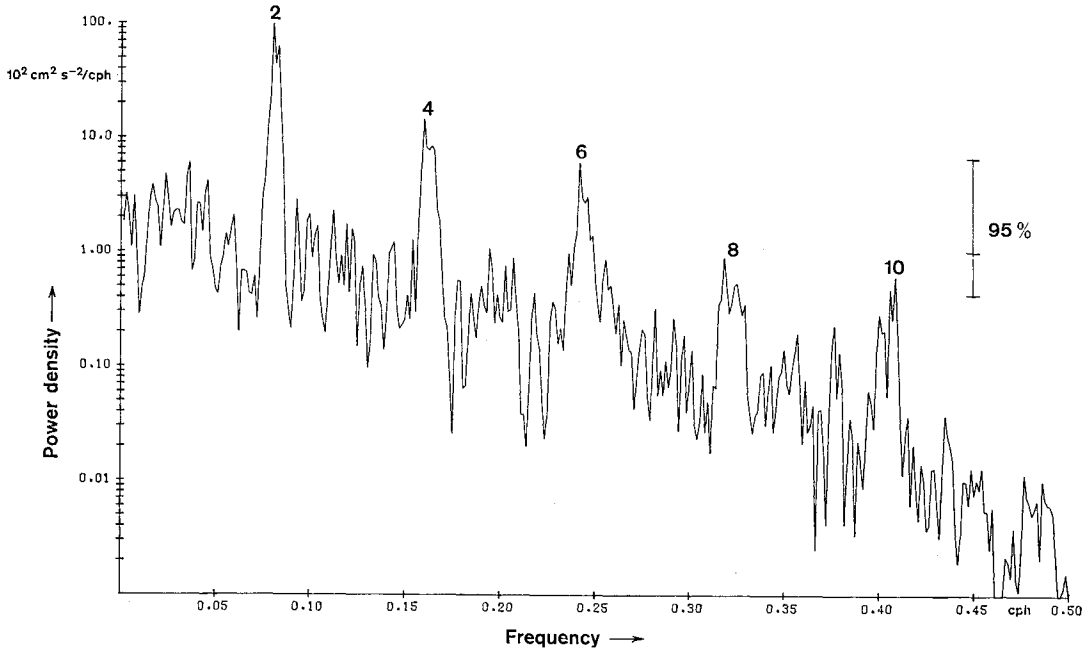

Fig. 15b (3)

of the v component is the residual energy significantly above the background for the odd bands. In the elevations the residual energy in the tidal bands is less significant, except for the tenth-diurnal band which stands out from the background noise; in the tidal analysis two constituents from this band, $4MS_{10}$ and $3M2S_{10}$ were included, but both contained very little energy.

For both the currents and elevations the residual energy in the diurnal band was very small compared with the background noise. Fig. 16 is a detailed plot of the power density at the low frequency end of the spectrum. It shows the absence of significant energy in the residuals for the diurnal band more clearly, and also shows the absence of significant energy in the currents at the inertial frequency. This lack of energy in the residuals within the diurnal tidal band is probably due to the virtual absence of shallow water energy, which is present in other bands and which is more difficult to include successfully in an analysis.

Fig. 16 also shows that the quasi-periodic oscillations revealed in Fig. 14 do not occur at any specific frequency, but are spread over a broad band. In the elevations there is a slight, but probably significant, energy minima between broad maxima centred around periods of 40 hours and 70 hours. The broad-band character of this residual spectrum is probably due to the broad-band character of the meteorological forcing. There is no evidence that natural periods of the North Sea are significant.

b) The progression of surges

Fig. 17 shows the cross spectrum of residuals for elevations and the v component of currents at the Inner Dowsing based on 324 days of simultaneous observations. There is cross-spectral energy in all of the even tidal bands. The current phases are more than 90^0 greater than the elevation phases up to about 0.20 cph indicative of a north to south wave progression. However, within the semi-diurnal band the residuals do not conform to this pattern although the tidal harmonics, which have already been removed are consistent with it. The significance of this for energy flux calculations will be discussed later. At frequencies above 0.20 cph the phase differences between elevation and current residuals are very variable due to the low energy in the cross-spectrum.

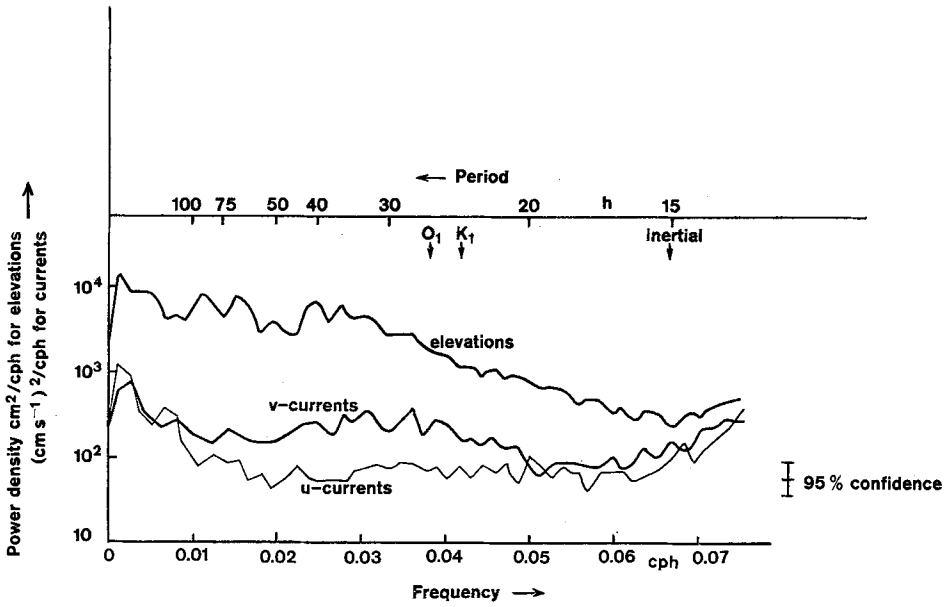

Fig. 16. Detailed power density plots for low frequency currents and elevations at the Inner Dowsing showing the absence of large residual energy within the diurnal band and at the inertial frequency, and the broad-band character of the long-period residual energy

c) Comparison of Inner Dowsing residuals with coastal residuals

Because meteorological influences on water movements are more effective in shallow water, and because of shallow-water tide generation, non-tidal residuals at coastal stations are expected to be greater than for stations off-shore. The Inner Dowsing elevation residuals have been compared with those at Hunstanton, which is at the mouth of the Wash, surrounded by extensive regions of shallow water.

Fig. 18 shows the power density of Hunstanton residuals based on analysis of 171 days of data between days 193/72 and 091/73. The energy level between the tidal bands is generally higher than at the Inner Dowsing and there is significant residual energy in both the odd and even tidal bands. Fig. 19 shows the coherence between the Hunstanton and Inner Dowsing elevation residuals up to a frequency of 0.25 cph. Long period residuals are highly coherent. Phases at Hunstanton are slightly greater than at the Inner Dowsing, consistent with north-south progression, and the least squares fitted line through the phases shows an increase of phase with frequency, consistent with shallow-water wave progression theory. However, within the semi-diurnal and fourth diurnal bands, the coherence is low showing that the residuals, after removing the highly correlated tidal signals, are not closely related between the Inner Dowsing and Hunstanton.

At frequencies greater than 0.25 cph the coherence is low and the phase differences are erratic.

For the 173 days of simultaneous data the total residual variance at the Inner Dowsing was 0.0351 m^2 while at Hunstanton the variance was 0.0499 m^2. Most of this variance, in both cases, was at low frequencies. Between zero and 0.033 cph the variance at the Inner Dowsing was 0.0267 m^2 and at Hunstanton 0.0334 m^2.

Table 9 extends this comparison of residual variance for a selection of stations along the British coast and within the Wash (Fig. 1 and 11). Where possible the data analysed was for the year 1972, but for the Wash stations the period was from July 1972 to August 1973. The Hunstanton variance for the extended period is greater than for the 173 days previously

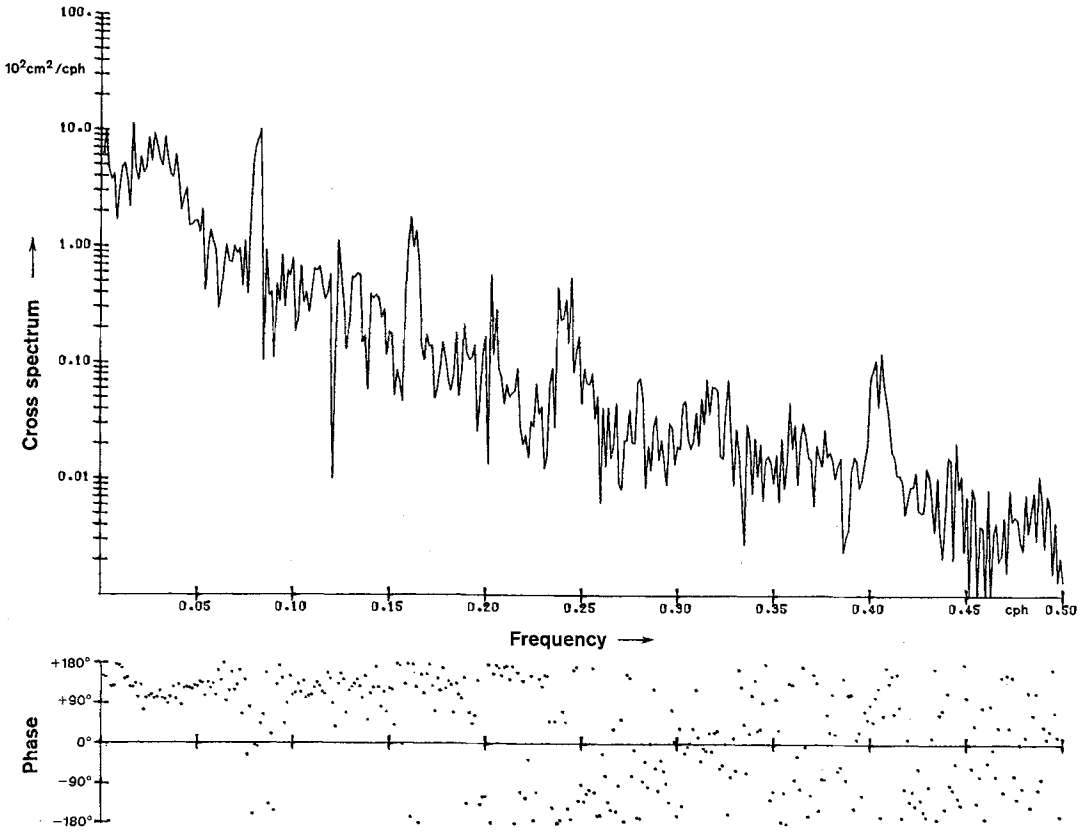

Fig. 17. Cross spectrum of elevations and v current residuals at the Inner Dowsing showing the north-south progression of long period waves

discussed. However, the residual variance for the Wash stations is not dramatically greater than at the Inner Dowsing. There is a general increase in the residual variance from north to south along the British coast. The residual variance at these ports is independent of the tidal range.

d) Surge-tide interaction

The interaction between surges and tides has been considered by several authors. Proudman [1955] has shown theoretically how bottom friction produces an interaction of tide and surge in an estuary. In this section we consider quantitatively the relationship between tidal and non-tidal elevations and currents for the year of data at the Inner Dowsing.

Consider each observed hourly value of elevation to consist of a tidal and a surge component:

$$O_\zeta = T_\zeta + S_\zeta. \tag{12}$$

As a first, visual check for interaction the O_ζ values have been plotted as dots in Fig. 20a, with the surge component as abscissa and the tidal component as ordinate. Figures 20b and 20c show the dot plots for the u and v components. The advantage of such a display is evident. For the elevations it is immediately apparent that the most frequently observed tidal levels are around ± 2.0 m, and that negative surges in excess of 0.8 m occur more often than similar positive surges. The u component of current has a distribution showing a tendency towards negative surges for a large positive tidal component, and positive surges for a large negative

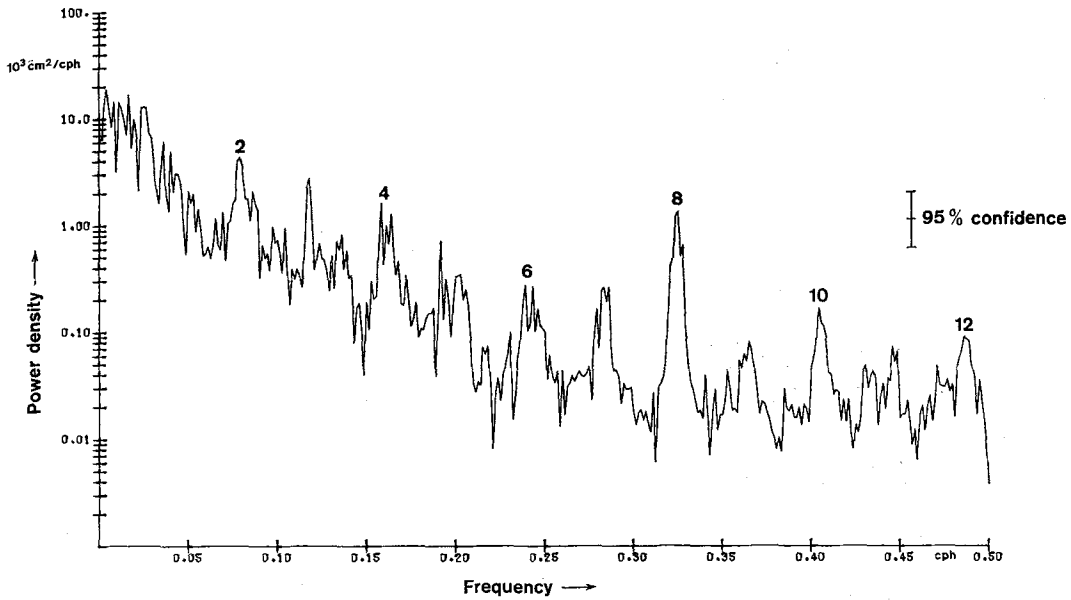

Fig. 18. Power density of Hunstanton elevation residuals showing the enhanced energy in the shallow-water tides compared with those at the Inner Dowsing

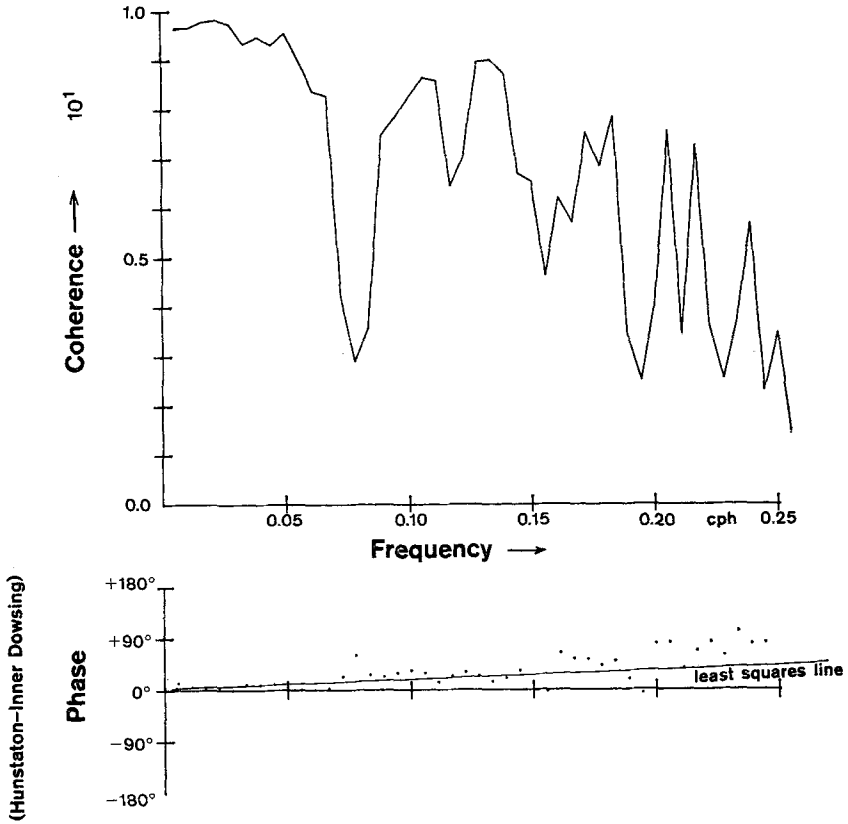

Fig. 19. Coherence and phase between Hunstanton and Inner Dowsing elevation residuals. Coherence is very high at low frequencies

tidal component. From our method of computing surges the implication of this is that extreme observed east-west currents tend to have a smaller amplitude than tidally predicted. The most frequent tidal currents along the axis are ± 0.20 m s^{-1}. This bi-modal distribution is less evident for the v current component, but in this case there is a greater frequency of southgoing than northgoing currents with amplitudes in excess of 0.8 m s^{-1}.

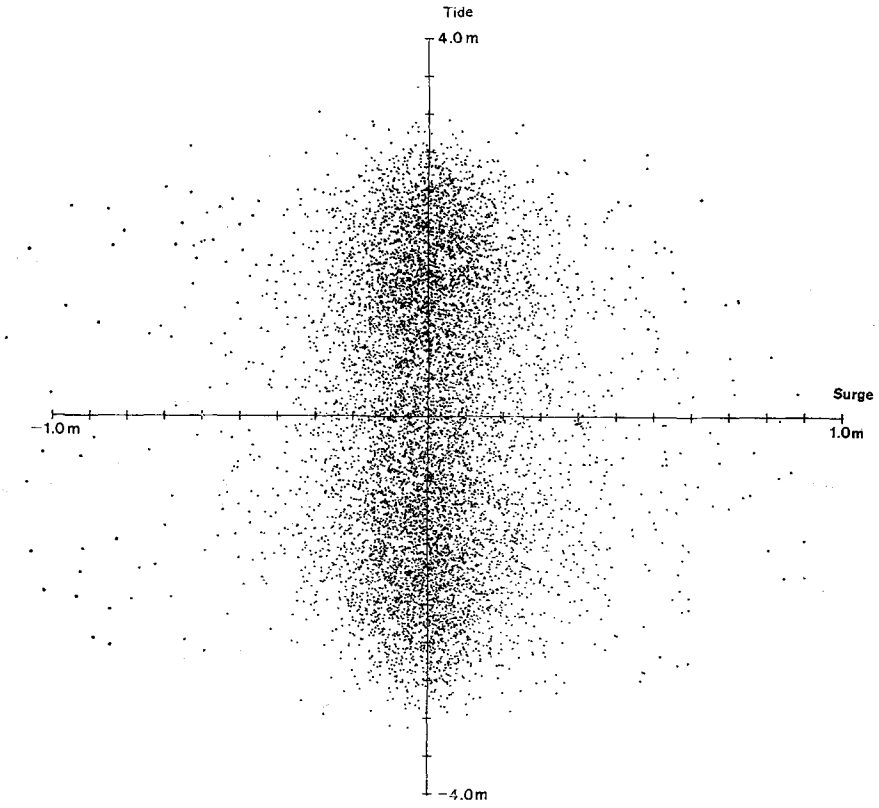

Fig. 20a

Fig. 20. Surge values plotted against simultaneous tidal values for the year of data at the Inner Dowsing. Surge-tide interaction would appear as an asymmetric surge distribution about the tidal axis

Table 10 contains a quantitative summary of the means and standard deviations of the surge distributions as a function of the corresponding tidal value. Overall mean values have been removed before tabulation. In all three cases the surge distributions are very little affected by the corresponding tidal value, but there are small but significant variations. In the elevations the standard deviation of the surges is greater at mid tide level than at the extreme levels so that extreme surges are less probable at the time of high or low water level. In the u-currents the largest non-tidal residuals occur at times of extreme currents, as is evident from Fig. 20b. For the v currents there is a systematic increase of the standard deviation from a minimum value for extreme northgoing tidal currents to a maximum value for extreme southgoing tidal currents, with the values for tidal currents of small amplitude approximately constant around 0.10 m s^{-1}.

e) Residual currents

The mean residual Eulerian flow throughout the year was in an approximately northwesterly direction (131°) at a speed of 0.039 m s^{-1}, in the opposite sense to the direction of tide and surge propagation. Figure 21 shows the residual drift from day 84/72 to day 138/72.

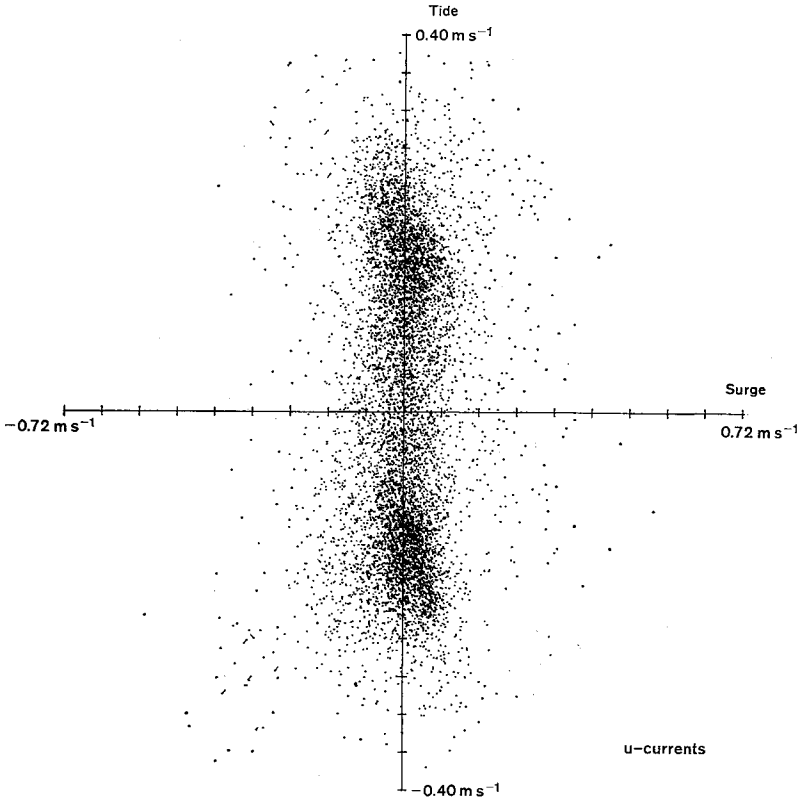

Fig. 20b

The change from this steady flow around day 98/72 occurred at a time of sustained winds from the south-west with an average speed of 16 m s^{-1} over several days. This north-westerly flow is also shown on the Admiralty atlas (1946) which gives a direction of 117° and a speed of 0.02 m s^{-1} at the Inner Dowsing light vessel position, 1 km south-east of the present tower. The same atlas shows a general south-easterly residual flow along the length of the coast from the River Tyne to the Thames Estuary.

This local reversal of the general residual flow pattern may be due to density gradients associated with a large fresh-water discharge from the Humber estuary. However, the Eulerian residual currents would be sensitive to any asymmetry in the tidal flow, as discussed earlier for the shallow-water tidal constituents. The vector dots of Fig. 10 must sum to a north-westerly residual vector. Although the Lagrangian flow of a single element of water need not be in a north-westerly direction, one of the keepers reported that a drift bottle thrown overboard from the tower was recovered at Spurn Head, north of the entrance to the Humber Estuary.

Table 11 summarises the residual currents measured at the other stations in the region.

f) Mean sea level changes

Because water levels are measured relative to a fixed point on the tower, any increase in mean water levels averaged over sufficiently long periods would indicate a sinking of the tower or a rise in mean sea level. To eliminate secular and seasonal variations of mean sea level, monthly mean values of mean sea level at Immingham which are related to a stable coastal datum, were compared with those at the tower. Fig. 22 shows the values of these differences over a period from October 1971, immediately after the tower was installed, to April 1973.

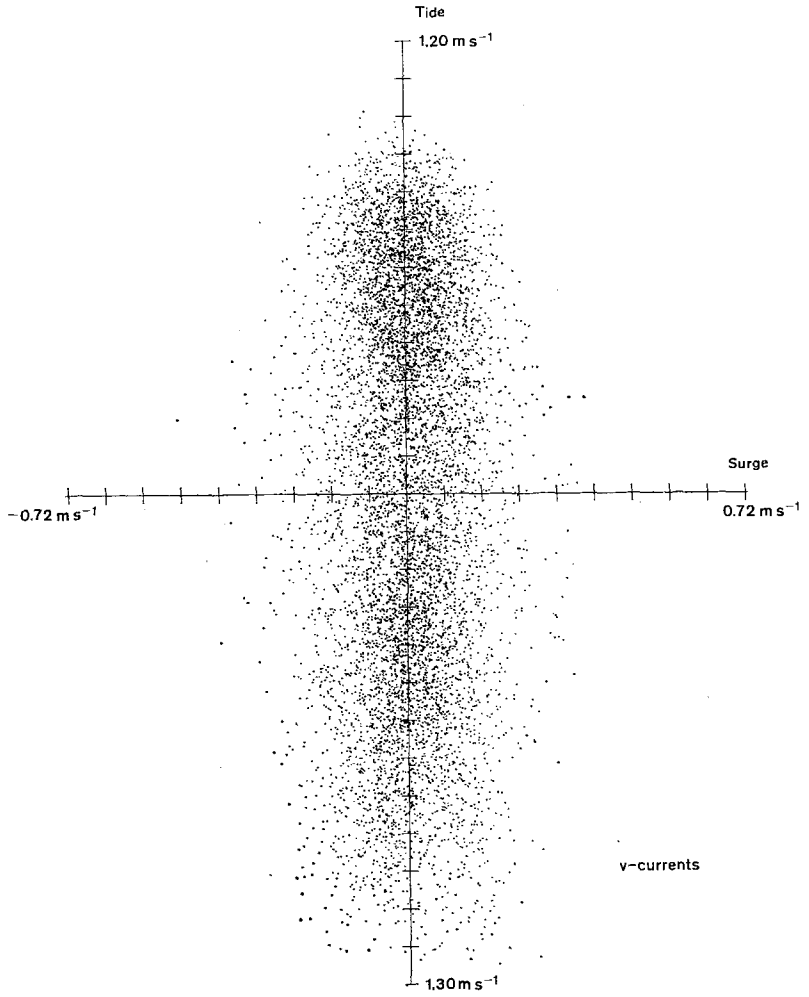

Fig. 20c

The lower graph shows the tilt of the tower in two orthogonal directions as measured by levelling instruments installed by Trinity House engineers.

Both the tilt and the mean level change during the first 3 months, but after this the tilts remain constant. However, the change in mean sea level shows a steady settling of the tower at a rate of approximately 0.08 m per year. Calculating the difference between levels at the Inner Dowsing and at Immingham assumes that oceanographic conditions do not vary, and in particular, that mean monthly residual currents across the line from Immingham to the tower are constant (see Alcock and Pugh [1975]).

Energy fluxes

Numerical computations by Prandle [1975] and by Flather [1976] have shown the southern North Sea and the Wash to be regions of relatively high frictional dissipation of tidal energy. We discuss the flux of energy through the Dowsing region for both tides and surges. We also consider the modulations of the energy flux at the Inner Dowsing during the spring-neap cycle.

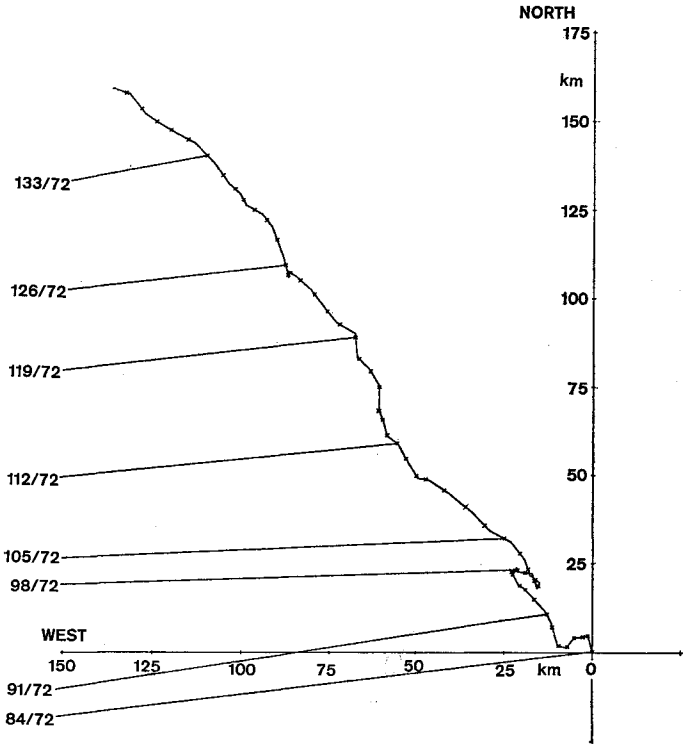

Fig. 21. Eulerian current residual drift measured at the Inner Dowsing tower, day 84/72 to day 138/72, showing average flow to the north-west at 0.04 m s^{-1}

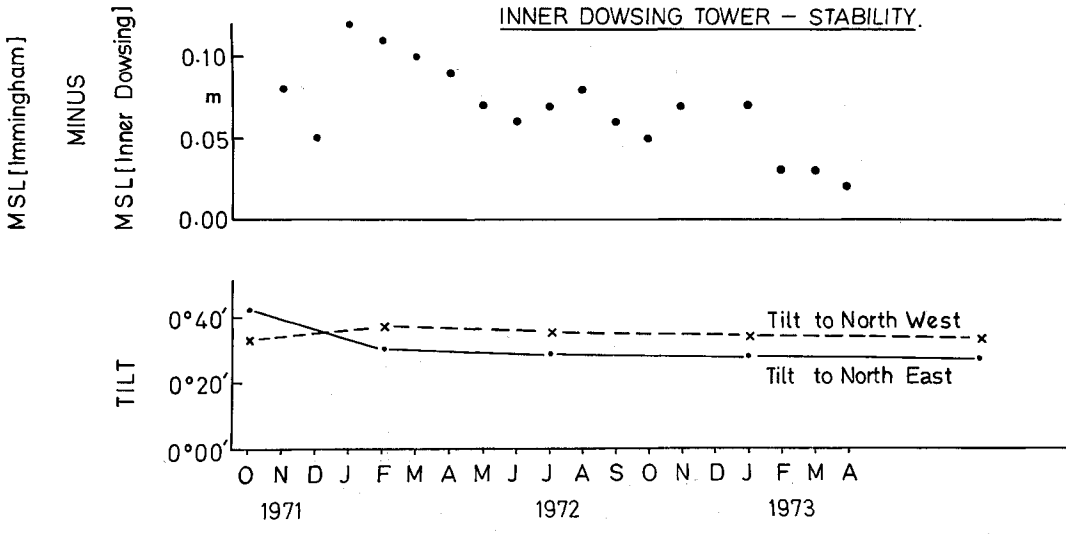

Fig. 22. Level and tilt stability of the Inner Dowsing tower, showing a gradual sinking of the tower at approximately 0.08 m per year

a) Mean energy fluxes in the region

The energy flux per unit length of section in time dt along the positive u-current axis is given by

$$u\rho\, dt \left\{ g d\zeta + \frac{1}{2}\left(2g\zeta^2 + (d+\zeta)\,(u^2+v^2) \right) \right\} \tag{13}$$

where d is the mean water depth,
ζ is the water level excursion from the mean level
and ρ is the water density.

This expression was first developed by Taylor [1919] in his computations of tidal friction for the Irish Sea. For most purposes, where the water level excursions are small compared with the mean depth, the second term may be ignored. For elevations and currents which vary harmonically:

$$\zeta = H \cos(\sigma t - g_\zeta) \quad u = U \cos(\sigma t - g_u)$$

the energy flux average over a tidal cycle is:

$$\tfrac{1}{2}\, \rho g d\, HU \cos(g_\zeta - g_u). \tag{14}$$

This may be extended to show that the energy fluxes for each tidal constituent may be added to give the total tidal energy flux. Consider the simple case of the principal lunar and solar constituents, M_2 and S_2:

$$\zeta = H_m \cos(\sigma t - g_m) + H_s \cos\left((\sigma + \Delta\sigma)\, t - g_s\right)$$
$$u = U_m \cos(\sigma t - g'_m) + U_s \cos\left((\sigma + \Delta\sigma)\, t - g'_s\right).$$

Substituting in the first term of (13) and multiplying we have:

$$\rho g d \{ H_m\, U_m \cos(\sigma t - g_m) \cos(\sigma t - g'_m) + H_s\, U_s \cos\left((\sigma + \Delta\sigma)\, t - g_s\right) \cos\left((\sigma + \Delta\sigma)\, t - g'_s\right) +$$
$$+ H_m\, U_s \cos(\sigma t - g_m) \cos\left((\sigma + \Delta\sigma)\, t - g'_s\right) +$$
$$+ H_s\, U_m \cos\left((\sigma + \Delta\sigma)\, t - g_s\right) \cos(\sigma t - g'_m) \}\, dt \tag{15}$$

and integrating over a complete spring-neap cycle, $t = 0$ to $t = \dfrac{2\pi}{\Delta\sigma}$:

$$\text{mean flux} = \rho g d \{ H_m\, U_m \cos(g_m - g'_m) + H_s\, U_s \cos(g_s - g'_s) \}$$

which is the energy flux of the two constituents independently calculated. This is analogous to the summation properties for the spectral decomposition of variance, and may be expanded by induction from the two constituent case to all harmonic constituents of different frequencies.

From (14) it is clear that the energy flux is zero in a standing wave, where $\cos(g_\zeta - g_u) = 0$. The flux is a maximum for a progressive wave because the maximum positive current occurs at high water. The direction of energy flux is therefore given by the direction of the progressive component in Table 6.

Table 12 summarises the results of computing the energy fluxes both numerically from the full expression (13), using actual or filtered observations, and the relationship (14) for a single constituent. Comparison of lines 1 and 2 for M_2 and $(M_2 + S_2)$ shows that 87.5 % of the total tidal energy flux is associated with the principal constituent M_2, and 97.2 % with the two principal constituents M_2 and S_2, where the computations are made over a full year. Line 5 is a computation of energy flux for the reduced period, for which good current meter data were available, and shows the stability of the result. Line 4 is the result of computing energy fluxes using only the first term of the full energy flux expression, and shows that the remaining terms make little contribution at the Inner Dowsing.

Line 6 is for the long period oscillations calculated by applying filter FLP08 to the currents and filter FLP04 to the elevations – see Fig. 13. The FLP08 filter was used for the current meter data, although it was not as efficient as FLP04, to avoid removing too much

data at the beginning and end of each current meter data block. The energy flux associated with these long periods is very small, 0.35% of the tidal energy flux, and of this 0.07% is attributable to the long period tidal terms, Sa, Ssa, Mm, Msf and Mf. The total energy flux vector associated with these five long period tides has an amplitude of 0.085 kW m^{-1} in a direction -83^0, the same direction as the total energy flux.

Line 8 gives the total energy flux computed from the unfiltered observations and so gives the total flux for both tides and surges together. This total energy is actually less than the sum of the tidal energy flux and the non-tidal flux computed separately. Because the energy fluxes in different frequency bands may be added vectorially, as shown above, this deficiency must be due to surge energy within the tidal bands. This may be interpreted as an interaction between the tidal variation of water level and current and the meteorological variations. These variations are coherent and appear in the cross-spectra between currents and elevations, but are not coherent within each separate time series, and so they are not removed by tidal analysis of the separate series. Furthermore, this interaction produces an energy flux vector which reduces the total energy flux.

Energy fluxes elsewhere in the region have been determined for periods of much less than a year (Table 12). Within the Wash the fluxes are small, but at Zo and the Shell-Esso platform the fluxes are comparable with the flux at the Inner Dowsing. Proudman and Doodson [1924] computed the energy flux at a position E_4 from a short period of observations. The value they obtained, which is given in the table for comparison, is close to the values determined in this paper using much longer periods of data.

b) Flux variations during a spring-neap cycle

Tidal energy is dissipated in the work done by the tidal currents against the frictional resistance of the sea bed. For unit area of sea bed, the frictional loss of energy equals the frictional stress times the water velocity at the bed. Empirically a stress of the form

$$-K\rho u \varrho$$

where K is a constant of the order of 0.0025
ϱ is the total current speed
u is a current component along the axis for which the stress is computed,
and ρ is the water density

has been found appropriate (Taylor [1919] has used this form for computations of energy budgets in the Irish Sea). For a rectilinear current the average dissipation per unit area taken over a tidal cycle is

$$\frac{4}{3\pi} K\rho W^3$$

where W is the amplitude of the harmonic variation of tidal current.

This dependence of energy dissipation on the cube of the tidal current amplitude poses an interesting problem. Taking the measurements of current at Station B in the Wash as an example, the harmonic amplitude is 0.64 m s^{-1} at spring tides ($M_2 + S_2$) and 0.30 m s^{-1} at neap tides ($M_2 - S_2$). The corresponding rates of dissipation of energy are 0.286 W m^{-2} and 0.029 W m^{-2}, so that the dissipation rate is greater by a factor of ten at spring tides. However, the energy flux from (14) varies as the product of the amplitudes of the tidal elevations and currents. At the Inner Dowsing the flux at spring tides, due to the variation in these amplitudes alone is 4.30 times the flux at neaps, suggesting that the energy dissipated during spring tides is substantially greater than the replenishing flux. Conversely the energy flux at neap tides is greater than the rate of dissipation.

There remains the possibility that shallow-water constituents, for example $2MS_2$, combine with M_2 and S_2 in such a way that the energy flux is enhanced at spring tides. For example, perhaps the phase angle $(g_\zeta - g_u)$ between elevation and current maxima adjusts during the spring-neap cycle to give a larger cosine term at spring tides. To investigate this possibility the hourly energy fluxes were computed for the year of observations directly from

the observational data, and then subjected to a harmonic analysis to determine the amplitude of the spring-neap flux i.e. at the Msf frequency. The result can be compared with the value for Msf obtained by an expansion of expression (15) in which the cross product of elevations and currents are synthesised as the sum of the M_2 and S_2 constituents. For the Msf term the expected amplitudes and phases are:

$$\text{Amplitude} = \sqrt{\gamma_1^2 + \gamma_2^2} \qquad \text{phase} = \arctan\left(\frac{\gamma_2}{\gamma_1}\right)$$

where

$$2\gamma_1 = H_m\, V_s \cos\,(g_s' - g_m) + H_s\, V_m \cos\,(g_s - g_m')$$

$$2\gamma_2 = H_m\, V_s \sin\,(g_s' - g_m) + H_s\, V_m \sin\,(g_s - g_m').$$

The observed and computed fluxes for Msf are in close agreement, showing that very little phase change occurs to modulate the energy flux. The harmonic energy flux vector during the spring-neap cycle which is plotted as an ellipse in Fig. 23, shows that the flux is closely

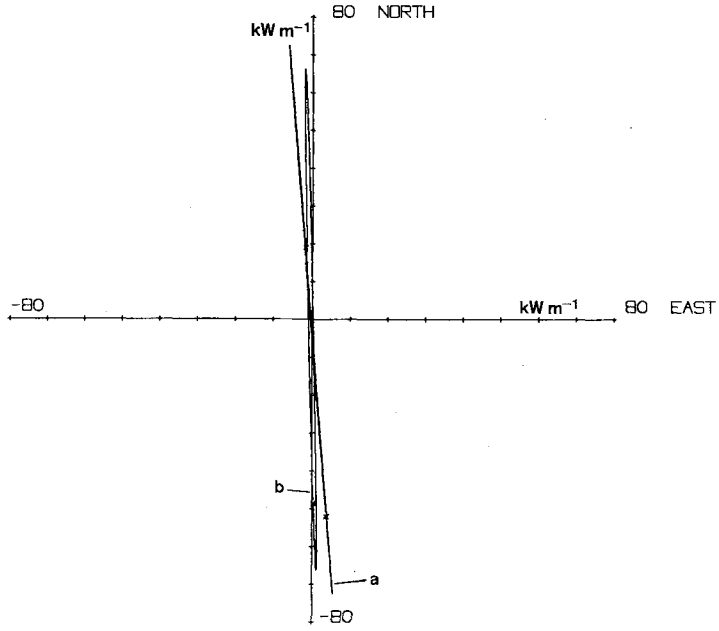

Fig. 23. Long period (Msf) energy flux for the Inner Dowsing a) from analysis of the hourly fluxes computed from the year of total current and elevation data and b) by combination of M_2 and S_2 alone. The two are not significantly different, which shows that the flux is proportional to the square of the tidal amplitude

rectilinear and that the flux at Msf from an analysis of a year of hourly fluxes is not significantly different from the flux at Msf calculated from a combination of M_2 and S_2 alone. Some other mechanism is necessary to resolve this paradox. Perhaps potential energy is stored during neap tides as an increase in mean level, and released later at spring tides. The energy budget during a spring-neap cycle requires a more detailed investigation, if possible, for a bounded region, such as the Irish Sea, which was used by G. I. Taylor in his original computations of energy flux during a semi-diurnal tidal cycle.

Conclusions

This paper presents the results of a detailed analysis of tides and surges in a complex coastal region of the North Sea. The principal conclusions may be summarised.

1. Pneumatic gauges are well suited for water level measurements from off-shore structures. Currents are more difficult to measure, but if the position of the meter is chosen to minimise the effect of the structure on the flow, then good results are possible.

2. The validity of tidal constituents based on analysis of a month of off-shore elevation or current data may be estimated from Table 2. Elevation constituents are generally more stable than the constituents of the current components. For analysis of short periods of data, current constituents may be related using the elevation relationships from a nearby port.

3. At the Inner Dowsing the astronomical current ellipses rotate in an anticlockwise direction whereas the shallow-water current ellipses rotate in a clockwise direction. This may be explained in terms of the non-rectilinear form of the measured flow. This non-rectilinear flow also explains the greater proportion of shallow-water variance in the current analyses compared with the proportion in the elevation analysis.

4. There is an annual modulation in the principal tidal constituent, M_2, which is not astronomical in origin, and which is coherent along the whole of the British coast of the North Sea.

5. Cotidal and coamplitude charts have been constructed for several tidal constituents, including the shallow-water constituents M_4, MS_4 and M_6. There is some evidence that M_4 and MS_4 behave as free waves over most of the region, whereas M_6 is forced by the M_2 tide.

6. The non-tidal residuals are not markedly smaller off shore than at coastal stations. Quasi-periodic long-period oscillations, travelling from north to south, have broad-band spectral characteristics.

7. The average energy flux due to tides and surges past the Inner Dowsing is 122.1 kW m^{-1} of section. 87.5% of this is due to the M_2 tide and only 0.45% is due to meteorological surges. Energy fluxes for each tidal constituent may be added vectorially. The energy flux varies as the square of the tidal amplitude.

Acknowledgements

An extended observational programme like the one reported here necessarily involves many people and skills. Within the Bidston Laboratory D. L. Leighton and A. J. Harrison and their colleagues were responsible for the preparation and deployment of the instruments. S. G. Loch and M. J. Howarth advised on the suite of programs for current meter data reduction. C. MacDonald and S. Brown supervised tide-gauge data reduction and C. M. Allen helped with the analyses. The Corporation of Trinity House provided facilities on the Inner Dowsing tower, and their light keepers were responsible for the efficient running of the tide gauge. Additional data was provided by the University of East Anglia, the Hydraulics Research Station, Wallingford, and Binnie and Partners, Consulting Engineers. The Conoco Oil Company provided helicopter facilities on numerous occasions.

Table 1

Summary of available data for the Dowsing region of the North Sea

IOS(B) is Institute of Oceanographic Sciences, Bidston Observatory. Data periods are given as the day number and year of the first and last observations

Station	Lat.	Long.	Approximate water depth below MSL	Data	Period	Instrumentation	Source
Inner Dowsing	53°19′N	00°35′E	20.0 m	Elevations	299/71 to 004/74 restarted 213/74	Pneumatic gauge (Neyrpic)	IOS(B)
				Currents	056/72 to 332/73	Aanderaa meter	IOS(B)
Roaring Middle	52°55′N	00°18′E		Elevations	July 1972 to November 1973	Pneumatic gauge (Neyrpic)	Binnie & partners and IOS(B). See Pugh & Waller [1975] — Wash Water Storage Scheme-feasibility study
Hunstanton	52°56′N	00°29′E		Elevations		,,	
West Stones	52°49′N	00°21′E		Elevations		,,	
Tabs Head	52°56′N	00°05′E		Elevations		,,	
Gibraltar Pt.	53°05′N	00°20′E		Elevations	198/72 to 228/72	Tide pole	Binnie
A	52°56′N	00°24′E	9.0 m	Currents	355/72 to 030/73	Plessey meter	H.R.S. Wallingford
B	52°57′N	00°20′E	12.0 m	Currents	354/72 to 030/73	Plessey meter	
Skegness	53°09′N	00°21′E		Elevations	258/73 to 337/73	Pneumatic gauge (Neyrpic)	IOS(B) — Joint North-Sea Data Acquisition Programme (1973)
Zo	53°20′N	01°14′E		Elevations	252/73 to 297/73	Offshore pressure capsule	IOS(B)
			23.0 m	Currents	250/73 to 293/73	Aanderaa meters	IOS(B)
Shell-Esso Field	53°05′N	2°08′E		Elevations	335/73 to 007/74	Digital float gauge	Min. Ag.
Platforms	53°05′N	2°11′E	36.0 m	Currents	242/73 to 271/73	Plessey meters	U.E. Ang.
Cromer	52°56′N	01°18′E		Elevations	256/74 to 287/74	Pneumatic gauge (Neyrpic)	IOS(B)
Immingham	53°38′N	00°11′ W		Elevations	1966 – 1 year	Float gauge	IOS(B) analysis files
Bull Sands Fort	53°34′N	00°04′E		Elevations	1966 – 1 year	Float gauge	
North Star Rig	53°42′N	02°05′E		Elevations	Feb/Mar 1966	Tide pole	
Great Yarmouth	52°34′N	1°44′E		Elevations	1942 – 1 year	Float gauge	I.H.B. Special pub. 26 No. 845
Lowestoft	52°28′N	1°45′E		Elevations	1965 – 1 year	Float gauge	IOS(B)

Table 2

Stability of Inner Dowsing tidal constituents for elevation and currents from monthly analyses

SD = standard deviation *SE* = standard error of the mean value = *SD*/(number of monthly analyses)$^{1/2}$

		H					*g*				
		mean	*SD*	*SE*	max	min	mean	*SD*	*SE*	max	min
O_1	ζ	0.177	0.012	0.004	0.194	0.149	114.0	7.3	2.1	123.9	98.3
	u	0.006	0.002	0.001	0.009	0.002	153.1	75.2	22.7	272.0	22.7
	v	0.045	0.008	0.002	0.061	0.032	232.2	13.3	4.0	248.1	199.6
K_1	ζ	0.149	0.012	0.003	0.171	0.140	285.3	6.0	1.7	298.5	274.1
	u	0.007	0.004	0.001	0.013	0.002	209.2	99.0	29.8	325.2	41.2
	v	0.040	0.008	0.002	0.051	0.031	45.8	7.6	2.3	55.7	31.4
N_2	ζ	0.376	0.012	0.004	0.392	0.349	139.4	3.4	1.0	144.2	133.6
	u	0.038	0.018	0.005	0.086	0.024	215.5	30.6	9.2	269.7	162.0
	v	0.130	0.031	0.009	0.191	0.085	278.5	22.5	6.8	328.9	252.1
M_2	ζ	1.969	0.029	0.008	2.011	1.919	162.2	1.0	0.3	163.5	160.5
	u	0.200	0.028	0.008	0.244	0.151	231.1	10.6	3.2	250.4	216.5
	v	0.693	0.056	0.017	0.767	0.592	304.0	11.3	3.4	322.3	290.1
S_2	ζ	0.682	0.010	0.003	0.698	0.667	208.5	1.8	0.5	210.6	204.1
	u	0.064	0.018	0.006	0.101	0.039	289.9	13.8	4.2	312.0	269.3
	v	0.237	0.025	0.008	0.270	0.201	345.6	13.1	3.9	7.3	331.2
M_4	ζ	0.035	0.004	0.001	0.041	0.028	242.3	8.9	2.6	256.0	229.9
	u	0.033	0.021	0.007	0.066	0.002	107.3	65.3	19.7	240.7	22.0
	v	0.065	0.012	0.004	0.084	0.039	30.1	20.0	6.0	65.2	5.1
MS_4	ζ	0.037	0.009	0.003	0.048	0.022	287.8	17.1	4.9	314.7	251.4
	u	0.021	0.015	0.005	0.049	0.007	155.8	62.7	18.9	273.6	54.9
	v	0.057	0.017	0.005	0.086	0.032	79.4	12.1	3.7	101.3	61.3
M_6	ζ	0.032	0.003	0.001	0.038	0.028	272.6	3.4	1.0	277.8	266.6
	u	0.021	0.011	0.003	0.046	0.009	138.4	37.7	11.4	200.4	90.5
	v	0.026	0.008	0.003	0.038	0.011	93.3	35.3	10.7	151.1	50.8

ζ = elevation in m
u = east-west components of current in m s^{-1}
v = north-south components of current in m s^{-1}
phases are in degrees relative to the equilibrium tide at Greenwich

Table 3

A comparison of the observed and the equilibrium tidal relationships between neighbouring constituents

(* indicates a principally shallow-water constituent)

Tidal species	Related	Reference	Amplitude ratio: Related reference				Phase: g (related) $-g$ (reference)			
			Elevations	u currents	v currents	Equilibrium tide	Elevations	u currents	v currents	Equilibrium tide
							degrees	degrees	degrees	degrees
1	P_1	K_1	0.27	0.82	0.31	0.33	−14.7	−9.7	−9.6	0.0
	π_1	K_1	0.04	0.48	0.08	0.02	−30.9	75.5	90.5	0.0
2	$2N_2$	N_2	0.16	0.17	0.18	0.13	−41.3	−108.2	−41.8	0.0
	μ_2*	N_2	0.07	0.49	0.10	—	65.2	69.0	−132.7	—
	ν_2	N_2	0.23	0.41	0.27	0.19	−5.1	−29.7	38.9	0.0
2	N_2	M_2	0.19	0.17	0.18	0.19	−22.8	−9.4	−37.7	0.0
	MKS_2*	M_2	0.004	0.01	0.12	—	179.4	−138.6	165.3	—
	L_2	M_2	0.04	0.05	0.05	0.03	3.3	−5.3	23.9	0.0
	S_2	M_2	0.34	0.32	0.35	0.46	46.3	62.6	42.7	0.0
2	T_2	S_2	0.05	0.12	0.02	0.06	−16.6	−54.7	85.0	0.0
	K_2	S_2	0.28	0.26	0.14	0.27	−3.4	−12.1	9.3	0.0
4	MS_4*	M_4	1.01	0.56	0.94	—	45.4	61.3	47.7	—
	MK_4*	M_4	0.32	0.29	0.08	—	40.6	42.5	37.1	—
6	$2MS_6$*	M_6	0.92	1.27	1.18	—	47.2	58.4	45.9	—

Table 4

Amplitudes and phases of the long-period tidal components at the Inner Dowsing
(standard errors for the observed values are shown in brackets)

		Elevations				Currents			
	speed	relative coefficient in astronomical tide ($M_2 = 100$)	observed amplitude	observed relative coefficient ($M_2 = 100$)	observed phase	east-west (u) amplitude	east-west (u) phase	north-south (v) amplitude	north-south (v) phase
	degrees per hour		m		degrees	m s^{-1}	degrees	m s^{-1}	degrees
M_m	0.5444	9.1	0.035 (0.008)	1.8	209 (13)	0.012 (0.003)	233 (13)	0.008 (0.002)	26 (16)
MS_f	1.0159	1.5	0.022 (0.005)	1.1	222 (13)	0.011 (0.003)	247 (13)	0.006 (0.002)	50 (16)
M_f	1.0980	17.2	0.023 (0.005)	1.2	159 (13)	0.002 (0.001)	263 (13)	0.003 (0.001)	324 (16)

Table 5

Summary of the sense of rotation of current ellipses within tidal bands

	Inner Dowsing	Zo	Shell Esso	Wash A	Wash B
Long-period	A	–	–	–	–
Diurnal	A	variable	variable	A	C
Semi diurnal	A	A	C	A	virtually rectilinear currents (clockwise)
Third diurnal	A (M_3) C	C	A	A	A
Fourth diurnal	C	C	A	A	A
Sixth diurnal	C	A	variable	C	C

C = clockwise rotation
A = anticlockwise rotation

Table 6

Progressive and standing wave amplitudes and directions

The standing wave direction is the direction of flow on the falling tide. Directions are measured positive anticlockwise from geographic east

		Progressive Wave amplitude	Progressive Wave direction	Standing Wave amplitude	Standing Wave direction
		m s^{-1}	degrees	m s^{-1}	degrees
Inner Dowsing	O_1	0.022	−85	0.040	89
	K_1	0.021	−100	0.036	93
	N_2	0.089	−87	0.091	69
	M_2	0.545	−82	0.453	66
	S_2	0.182	−88	0.288	33
	M_m	0.013	−36	0.005	175
	MSf	0.011	−34	0.005	169
Zo	M_2	0.600	−44	0.280	90
Shell-Esso platform	M_2	0.615	−70	0.480	−97
Wash station A	M_2	0.045	7	0.600	58
Wash station B	M_2	0.008	132	0.450	79

Table 7

Comparison of observed and astronomical H_1 and H_2 constituents in elevation measurements along the coast of Britain. H_1 and H_2 are the constituents which produce an annual modulation of M_2

		Observed		Astronomical		Non-astronomical (O – A)	
		H	*g*	*H*	*g*	*H*	*g*
		m	degrees	m	degrees	m	degrees
Lerwick	H_1	0.0018	97.8	0.0020	311.5	0.0036	115.5
	H_2	0.0024	23.9	0.0018	311.5	0.0025	65.7
Wick	H_1	0.0107	224.6	0.0035	322.3	0.0117	207.2
	H_2	0.0033	147.9	0.0031	322.3	0.0064	145.2
Buckie	H_1	0.0123	311.1	0.0041	338.1	0.0088	298.7
	H_2	0.0144	126.9	0.0036	338.1	0.0176	133.0
Invergordon	H_1	0.0120	220.5	0.0047	336.9	0.0147	203.8
	H_2	0.0036	142.5	0.0041	336.9	0.0076	150.2
Aberdeen	H_1	0.0286	329.1	0.0045	23.8	0.0263	321.2
	H_2	0.0157	195.1	0.0040	23.8	0.0196	196.9
North Shields	H_1	0.0207	1.5	0.0055	87.7	0.0211	343.4
	H_2	0.0195	264.5	0.0048	87.7	0.0243	265.1
Immingham	H_1	0.0480	98.2	0.0079	163.4	0.0453	89.3
	H_2	0.0152	49.0	0.0069	163.4	0.0191	29.9
Inner Dowsing	H_1	0.0309	97.7	0.0068	162.2	0.0286	85.3
	H_2	0.0213	320.3	0.0060	162.2	0.0270	325.1
Lowestoft	H_1	0.0071	205.5	0.0025	259.3	0.0060	185.8
	H_2	0.0060	9.5	0.0022	259.3	0.0071	26.4
Harwich	H_1	0.0295	289.5	0.0046	328.5	0.0261	283.2
	H_2	0.0026	264.4	0.0041	328.5	0.0038	186.5
Southend	H_1	0.0437	313.9	0.0077	353.2	0.0381	306.6
	H_2	0.0028	186.2	0.0063	353.2	0.0091	176.0

Table 8

Effects of the H_1 and H_2 modulating constituents on tidal times and ranges

Port	Time of HW and LW				Range			
	Later by	Month	Earlier by	Month	Greater by	Month	Less by	Month
	min		min		cm		cm	
Lerwick	2	March	1½	July	1	Sept	1	March
Aberdeen	4	July	4	Feb	6	July	4	Jan
Immingham	4	Sept	3	Feb	6	June	4	Jan

Table 9

Comparison of non-tidal residual variance and standard deviations for elevations at several ports on the British coast of the North Sea, for comparison with the off-shore residuals at the Inner Dowsing

Location	Period	Original variance	No of harmonic constituents in analysis	Residual variance	Standard deviation
		m^2		m^2	m
Buckie	1972	0.841	62	0.0213	0.146
Invergordon	1972	1.117	62	0.0256	0.160
North Shields	1972	1.488	62	0.0246	0.157
Lowestoft	1972	0.343	62	0.0331	0.182
Harwich	1972	1.034	62	0.0335	0.183
Southend	1972	2.412	62	0.0404	0.201
Roaring Middle	July 1972 to	3.441	62	0.0420	0.205
Hunstanton	August 1973	3.098	62	0.0552	0.235
West Stones	(with gaps)	2.236	62	0.0495	0.222
Tabs Head		3.360	62	0.0353	0.188
Inner Dowsing	1972	2.307	100	0.0355	0.1884
			62	0.0359	0.1895
			60 (H_1 and H_2 excluded)	0.0363	0.1905

Table 11

Residual currents at stations in the Dowsing region

Station	Period	Mean speed	Direction (degrees anticlockwise from east)
		$m\ s^{-1}$	degrees
Inner Dowsing	056/72 to 078/73	0.039	131
Wash A	355/72 to 030/73	0.090	−162
Wash B	354/72 to 030/73	0.049	114
Zo	250/73 to 279/73	0.015	−96
Shell-Esso platform	242/73 to 271/73	0.074	122

Table 10

Tide-surge interaction statistics showing the surge elevations and current components at the Inner Dowsing as a function of the simultaneous tidal elevations and currents

	Elevations				East-West Currents				North-South Currents			
	Tide Level	Total	Mean Surge	Standard deviation	Tidal Current	Total	Mean Surge	Standard deviation	Tidal Current	Total	Mean Surge	Standard deviation
	m		m	m	m s^{-1}		m s^{-1}	m s^{-1}	m s^{-1}	m s^{-1}	m s^{-1}	m s^{-1}
1												
2												
3												
4												
5									1.05	1	–	–
6	3.17	1	–	–					0.95	33	−0.021	0.052
7	2.83	39	−0.011	0.106					0.85	184	−0.003	0.076
8	2.50	189	0.016	0.135	0.375	16	−0.016	0.134	0.75	436	−0.006	0.081
9	2.17	411	−0.004	0.169	0.325	57	−0.022	0.117	0.65	555	0.001	0.084
10	1.83	560	−0.001	0.164	0.275	225	−0.013	0.094	0.55	547	0.002	0.085
11	1.50	650	−0.004	0.174	0.225	531	−0.011	0.081	0.45	557	0.006	0.092
12	1.17	720	0.002	0.175	0.175	957	0.003	0.064	0.35	506	0.006	0.092
13	0.83	627	0.001	0.183	0.125	823	0.016	0.065	0.25	426	0.010	0.106
14	0.50	527	0.003	0.187	0.075	633	0.008	0.072	0.15	402	0.001	0.105
15	0.17	478	0.010	0.197	0.025	523	−0.001	0.075	0.05	388	0.009	0.111
16	−0.17	486	−0.007	0.189	−0.025	560	0.000	0.082	−0.05	351	−0.009	0.101
17	−0.50	501	0.006	0.207	−0.075	681	−0.003	0.079	−0.15	399	0.004	0.102
18	−0.83	555	−0.009	0.200	−0.125	1125	−0.001	0.065	−0.25	395	0.006	0.099
19	−1.17	631	−0.003	0.176	−0.175	1043	0.001	0.072	−0.35	480	0.011	0.100
20	−1.50	659	0.004	0.201	−0.225	442	−0.006	0.089	−0.45	447	−0.002	0.097
21	−1.83	629	−0.003	0.185	−0.275	114	−0.025	0.145	−0.55	433	0.001	0.095
22	−2.17	545	−0.009	0.173	−0.325	36	−0.018	0.165	−0.65	343	−0.003	0.100
23	−2.50	347	−0.004	0.162	−0.375	6	−0.152	0.198	−0.75	301	−0.008	0.096
24	−2.83	181	0.023	0.154					−0.85	245	−0.007	0.098
25	−3.17	46	−0.014	0.135					−0.95	188	−0.011	0.106
26	−3.50	2	−0.099	–					−1.05	101	−0.019	0.119
27									−1.15	43	0.008	0.121
28									−1.25	14	0.042	0.127
29												
30												

Table 12

Amplitudes and directions of energy fluxes a) for various frequency bands and by various methods over a long period at the Inner Dowsing, and b) for M_2 and S_2 numerically over short periods elsewhere in the region

Directions are measured positive anticlockwise from east. Mean water depths, where appropriate are given in Table 1. E_4 is from the Proudman and Doodson [1924] computations for comparison

Station	Constituents	Computed using G. I. Taylor expression for single harmonic constituents		Computed numerically from observations using full G. I. Taylor expression		Total days for numerical computations
		kW m^{-1}	degrees	kW m^{-1}	degrees	
Inner Dowsing	1. M_2	108	−82			
	2. $M_2 + S_2$	120	−83			
	3. All tidal – full yr			123.4	−83.6	366
	4. All tidal – 1st term of expression only			122.0	−83.3	324
	5. All tidal – full expression			122.0	−83.5	324
	6. Long period tides and surges			0.44	−41	277
	7. All surges			0.55	−49	324
	8. Total tides + surges			122.1	−83.8	324
Wash Station A	M_2	9	− 8	10	−53	37
Wash Station B	M_2	1	−16	3	−16	37
Zo	M_2	106	−44	125	−44	34
Shell-Esso platform	M_2	83	−70			
E_4 53°34′N 0°59′E (Proudman & Doodson, [1924])	M_2	103	−63			

References

Alcock, G. A. and D. T. Pugh, 1975: Hydrodynamic levelling of an off-shore tide gauge. Proc. Instn civ. Engrs, Part 2, **59,** 123–137.

Cartwright, D. E., 1968: A unified analysis of tides and surges round north and east Britain. Philos. Trans. r. Soc. (A) **263,** 1–55.

Cartwright, D. E. and R. J. Tayler, 1971: New computations of the tide-generating potential. Geophys. J. R. astr. Soc. **23,** 45–74.

Cartwright, D. E., W. Munk and B. Zetler, 1969: Pelagic tidal measurements. Trans. Amer. geophys. Un. **50,** 472–477.

Corkan, R. H., 1934: An annual perturbation in the range of tide. Proc. R. Soc. (A) **100,** 305–329.

Darbyshire, J. and M. Darbyshire, 1956: Storm surges in the North Sea during the winter 1953–4. Proc. R. Soc. (A) **235,** 260–274.

Flather, R. A., 1976: A tidal model of the north-west European continental shelf. Mem. Soc. Sci. Liège. **9.** [In press].

Hydrographic Department, Great Britain, 1946: Atlas of tides and tidal streams, British Isles and adjacent waters. 4th edition. Chart 5057.

Oberkommando der Kriegsmarine, 1942: Karten der harmonischen Gezeitkonstanten für das Gebiet der Nordsee. Ausgabe A, Nr. 2752. Hrsg. (Bearb.): Marineobservatorium Wilhelmshaven.

Proudman, J. and A. T. Doodson, 1924: The principal constituent of the tides of the North Sea. Philos. Trans. r. Soc. (A) **224,** 185–219.

Proudman, J., 1955: The effect of friction on a progressive wave of tide and surge in an estuary. Proc. R. Soc. (A) **233,** 407–418.

Prandle, D., 1975: Storm surges in the southern North Sea and River Thames. Proc. R. Soc. (A) **344,** 509–539.

Pugh, D. T., 1972: The physics of pneumatic tide gauges. Int. hydrogr. Rev. **49,** 71–97.

Pugh, D. T. and W. R. Waller, 1975: Sea-level measurements in the Wash Bay. Proceedings of the 14th Coastal Engineering Conference, Copenhagen, June 1974, published by the American Society of Civil Engineers, March 1975, 2519–2538.

Ramster, J. W. and M. J. Howarth, 1975: A detailed comparison of the data recorded by Aanderaa Model 4 and Plessey MO21 recording current meters moored at two shelf-sea locations. Dt. hydrogr. Z. **28,** 1–25.

Taylor, G. I., 1919: Tidal friction in the Irish Sea. Philos. Trans. r. Soc. (A) **220,** 1–93.

Eingegangen im Juli 1976

Anschrift der Verfasser:
D. T. Pugh, J. M. Vassie, Institute of Oceanographic Sciences, Bidston Observatory, Birkenhead, Merseyside, England